


How Properties that Distinguish Solids from Fluids and Constraints of Spherical Geometry Suppress Lower Mantle Convection

Anne M. Hofmeister¹, Everett M. Criss²

1. Department of Earth and Planetary Sciences, Washington University, St. Louis, MO 63130, USA

2. Panasonic Avionics Corporation, Lake Forest, CA 92630, USA

 Anne M. Hofmeister: <http://orcid.org/0000-0002-4100-0504>

ABSTRACT: The large magnitude of the dimensionless Rayleigh number ($Ra \sim 10^8$) for Earth's $\sim 3\,000$ km thick mantle is considered evidence of whole mantle convection. However, the current formulation assumes behavior characteristic of gases and liquids and also assumes Cartesian geometry. Issues arising from neglecting physical properties unique to solids and ignoring the spherical shapes for planets include: (1) Planet radius must be incorporated into Ra , in addition to layer thickness, to conserve mass during radial displacements. (2) The vastly different rates for heat and mass diffusion in solids, which result from their decoupled transport mechanisms, promote stability. (3) Unlike liquids, substantial stress is needed to deform solids, which independently promotes stability. (4) High interior compression stabilizes the mantle in additional minor ways. Therefore, representing conditions for convection in solid, self-gravitating spheroids, requires modifying formulae developed for bottom-heated fluids near ambient conditions under an invariant gravitational field. To derive stability criteria appropriate to solid spheres, we use dimensional analysis, and consider the effects of geometry, force competition, and microscopic behavior. We show that internal heating has been improperly accounted for in the Ra . We conclude that the lower mantle is stable for two independent reasons: heat diffusion far outpaces mass diffusion (creep) and yield strength of solids at high pressure exceeds the effective deviatoric stress. We discuss the role of partial melt in lubricating plate motion, and explain why the Ra is not applicable to the multi-component upper mantle. When conduction is insufficient to transport heat in the Earth, melt production and ascent are expected, not convection of solid rock.

KEY WORDS: plasticity, diffusion, mantle convection, stability criteria, dimensional analysis, geometry.

0 INTRODUCTION

Dimensional analysis is commonly utilized in fluid dynamics due to the complexity of the problems encountered. The Raleigh number (Ra) plays a pivotal role in studies of natural (free) convection (e.g., Tritton, 1977), and is an essential variable in non-dimensional numerical simulations of mantle convection (e.g., Zhong et al., 2015; Schubert et al., 2001). The classical dimensionless number that Rayleigh (1916) derived for fluids in a box in a uniform gravity field is

$$Ra = \frac{\alpha \Delta T g h^3}{\kappa \nu} \quad (1)$$

where α is volumetric thermal expansivity, ΔT is the temperature difference across the system, g is the constant gravitational acceleration, κ is thermal diffusivity, and ν is kinematic viscosity,

*Corresponding author: hofmeist@wustl.edu

© China University of Geosciences and Springer-Verlag GmbH Germany, Part of Springer Nature 2017

Manuscript received June 11, 2017.

Manuscript accepted November 13, 2017.

which is related to dynamic viscosity ($\mu = \rho \nu$ where ρ is density). Modifications to Ra made in geodynamic studies are minor (Sec. 1) and little affect the calculations presented in this introduction.

High estimates of Ra ($\sim 10^8$) for Earth's whole mantle (the rocky, outermost $\sim 2\,890$ km) is considered evidence for whole mantle convection. The immensity of these values largely results from h being large and cubed in Eq. (1). For comparison, we calculate Ra for Earth's lithosphere. The continental lithosphere is ~ 150 km thick with $\Delta T \sim 1\,000$ K. Continental rocks are insulating with $\kappa \sim 0.5$ mm²·s⁻¹ (Whittington et al., 2009). From the review of Bürgmann and Dresen (2008), geodetic data on continental lithosphere gives $\mu < 10^{20}$ Pa·s. Their upper limit is compatible with laboratory data on dry and cold material, which represents the highest possible lithosphere viscosity. Much lower values (10^{16} Pa·s) have been considered for the deepest regions. Using this upper limit, along with typical values of $\rho = 2\,500$ kg·m⁻³, $\alpha_v = 3 \times 10^{-5}$ K⁻¹ and $g = 9.8$ m·s⁻² sets a minimum for Ra of $> 50\,000$ for the continental lithosphere, which is far above the critical value of $\sim 1\,700$. Yet, this layer does not convect.

Hence, estimates of supercritical Ra are insufficient evidence for whole mantle convection, especially insofar as the

modeled material is not a fluid. Instead, this region is a chemically and physically layered combination of fluid and solid constituents, with measurable motion of its uppermost solid plates. The Ra argument cannot be invoked to describe the motions observed in the upper mantle (UM) and transition zone (TZ), because it is inapplicable due to unequivocal layering in this region. Specifically, the lithosphere is underlain by a thick (~180 km) weak, low velocity zone partially consisting of lubricating, low viscosity melt (for basalt, $\nu \sim 0.2 \text{ m}^2 \cdot \text{s}^{-1}$; Hofmeister et al., 2016). Additionally, the chemical composition of the lithosphere differs from both the oceanic crust and the asthenosphere, which are solid and non-homogeneous.

Researchers producing convection models acknowledge that attributing plate tectonics to whole mantle convection involves several first-order difficulties, such as what the mechanism is, how a weak energy source can drive convection, whether mantle plumes exist, and how the known chemical heterogeneities in the UM+TZ can persist (Bercovici, 2015). These problems bear crucially on the hypothesis of lower mantle (LM) involvement, which has been debated for decades because of inadequate supporting evidence, as detailed in Sections 0.1 and 0.2. A lack of seismological evidence for deep plumes is particularly troublesome, because plumes are a hallmark of all demonstrably convecting systems. See Foulger (2010) for additional discussion of the plumes controversy.

0.1 Evidence for Lower Mantle Stability

For $Ra \sim 10^8$, heat transfer is expected to be $\sim 300\times$ conductive per correlations of Ra with the Nusselt number where $Nu = \text{total flux}/\text{conductive flux}$ (e.g., Davies, 2011; Tritton, 1977; Elder, 1976). However, large Nu is not compatible with the available information on Earth's current heat flux, as follows: Measurements of surface heat flux provide 28 TW, whereas models consider higher values of 46 TW (summarized by Hamza, 2013). The higher model value allegedly includes primordial heat, flux from the core mantle boundary, and addresses hydrothermal circulation (e.g., Davies, 2011; Stein and Stein, 1992), but these additions likely result in heat flux overestimation (Criss and Hofmeister, 2016; Hofmeister and Criss, 2005). Measured values overlap with meteoritic estimates of interior heat production of 20–30 TW (e.g., Lodders, 2000). For model or measurement, dividing the surface output by the estimated interior production provides $Nu < 2.3$, which value vastly differs from $Nu \sim 300$ suggested from the estimates of Ra. Per experiments and theory (e.g., Koschmieder and Pallas, 1974), stability or weak convection is expected for such low Nu. Furthermore, a conductive or weakly convective state for Earth's mantle is also supported by geologic evidence: neither the style of surface motions, nor the temperatures, nor the chemical compositions of magmas have changed significantly over the last 20% of Earth's history (Hamilton, 2011). During this same $\sim 10^9$ year interval, interior radioactive heat production has decreased very slowly (van Schmus, 1995). Furthermore, conductive cooling models, which cover a wide range of mantle conditions, are also consistent with a surface heat flux of 10–40 TW (Criss and Hofmeister, 2016).

The motions of the lithospheric plates are considered evidence for internal motions, although the mechanism is not un-

derstood (Bercovici, 2015). Importantly, circulation is a first-order attribute of convection. Current mantle convection models do not address either the predominantly east-west motion of the plates, or that 670 km is the maximum depth for many plates (Doglioni and Panza, 2015). The manner in which the plates move (hinge rollback) is incompatible with lower mantle involvement (Hamilton, 2002) and is inconsistent with simple circular motions. Average plate velocities of $\sim 4 \text{ cm} \cdot \text{y}^{-1}$, show that the period of whole mantle overturn must be immense ($\sim 1/4$ Ga) if circulation occurs. This value is a substantial fraction of the Earth's age (4.5 Ga) and is an even greater fraction of the ~ 1 Ga interval when plate tectonics clearly operated (Hamilton, 2011). Therefore, plate velocities corroborate the weak and sluggish system suggested by the heat flux. Furthermore, many seismologic investigations show that activity is limited to the upper mantle. Seismic studies of the Iceland region show that low-wave-speed anomalies associated with upwelling are confined to the upper mantle (Du et al., 2006; Foulger et al., 2001). The same is true for the Yellowstone region (Gao and Liu, 2014) and the European Cenozoic rift (Fichtner and Villaseñor, 2015). The foci of earthquakes are all above 670–690 km (Rees and Okal, 1987). Similarly, even diamonds with metal inclusions appear to originate in the transition zone (Smith et al., 2016). Phase equilibria suggest origination is above 670 km (Gasparik, 2000). All of these observations suggest that the lower mantle (670 to 2 890 km depths) does not participate in mantle circulation.

In summary, a large body of independent observations support circulation being weak and limited to the UM+TZ. Support for lower mantle circulation is limited to the Ra number being large, the interpretation of seismic tomography images as plates penetrating into the lower mantle, and seismological evidence for broad features deep in the lower mantle (French and Romanowicz, 2015). However, these features are not tall and thin, as “plumes” are envisioned, and about one third of the slabs are flat lying (Goes et al., 2017). Furthermore, Foulger et al. (2013) have argued that tomographic images of descending plumes are over interpreted.

0.2 Problems in Representing the Complex Earth

Earth is layered, which is not addressed in the Ra. Discontinuities in the seismic velocities at 410 and 670 km are interpreted as phase transitions, but such assignments assume that the upper and lower mantles have the same chemical composition (Agee, 1998). In contrast, isotopic evidence conclusively shows that the UM+TZ, from whence geological samples originate, is demonstrably chemically heterogeneous. Recent studies point to chaotic distribution (Armienti and Gasperini, 2010).

Layering involves Earth's heat producing elements, whereby U and Th are almost entirely located in the continental crust (Henderson, 1982). This configuration is incompatible with whole mantle convection, although lateral flow of heat from deep continental roots might affect the upper mantle. To address the problematic absence of bottom heating, additional deep heat sources, such as latent heat released during freezing of the iron core, have been suggested (e.g., Stacey and Stacey, 1999). Primordial heat of accretion or core formation has been considered substantial based on geoneutrino data (Gando et al., 2011). How-

ever, this method only detects U and Th decay events, which are dominated by nearby continental crust and nuclear reactors, and in assuming the contribution from K from the mantle also assumes its primordial heat (Hofmeister and Criss, 2013). Isothermal conditions are expected for the two-phase core, because any receipt of heat (internal or external) will change the relative proportions of solid and liquid, but not the temperature, as is shown by the well-known thermodynamic analysis of ice bath behavior (Criss and Hofmeister, 2016). The amount of primordial heat cannot be large, considering the energy stored in Earth's spin, and the energy used to create its ordered, layered state (Hofmeister and Criss, 2015, 2012). That the measured surface flux equals, within uncertainty, the meteoritic estimates for radioactive emissions suggests that primordial heat has created the high temperatures of Earth's deepest interior, rather than being shed to space (Criss and Hofmeister, 2016).

Finally, we note that similarly sized Venus has a surface which differs considerably from that of Earth, by appearing old, with no evidence for plate tectonics (Hamilton, 2015). Venus' spin rate differs from that of Earth, and moreover, Earth's spin plays an important role in the particulars of plate motions (Doglioni and Anderson, 2015). Clearly, behavior inside a planet is far more complex than that of homogeneous fluid in a box, which the Ra number describes.

0.3 Purpose and Organization of the Paper

Vigorous whole mantle convection, as suggested by the entire mantle's high Rayleigh number, conflicts with virtually all pertinent observations as described above. The above discussion of Ra for continental lithosphere shows that a supercritical Ra is insufficient evidence of convection. Moreover, using Ra as a parameter in numerical models (e.g., Zhong et al., 2015; Schubert et al., 2001) means that these model outcomes largely rest on Ra accurately portraying mantle behavior. Whether this portrayal is accurate is a concern, because conditions considered in the historic derivation of the Rayleigh number obviously differ from those in Earth's mantle. No previous study has appreciably explored the limitations of the classical Rayleigh number in regard to its application to planets.

Therefore, the present paper focuses on the physical basis for the Ra. Section 1 provides background information on dimensional analysis, and shows that existing modifications to the classical Ra number inadequately address conditions in planets. Section 2 shows that the effect of spherical geometry on Ra is independent of any changes needed to address how properties of solids differ from those of liquids. Section 3 proposes stability criteria for solids based on thermodynamic principles, continuum mechanics, and dimensional analysis. From our formulae and considering available data on the relevant parameters, stability of the lower mantle is expected (Sec. 4). Section 5 briefly covers why plate tectonics may not require upper mantle convection, although resolving this issue is beyond the scope of the present paper.

1 DIMENSIONAL ANALYSIS

1.1 Method

To determine whether all factors needed to ascertain convective instability of planets are included in Eq. (1) requires

understanding the method of dimensional analysis. This section summarizes this method and describes the dimensionless numbers associated with convection.

For any problem, the number of pertinent dimensionless groups (termed " π 's") is the difference between the numbers of relevant variables and distinct unit-dimensions (Buckingham, 1914). In a "classical" analysis of fluid flow (Table 1, top), the number of π 's is 4=9 variables less 5 unit-dimensions. To determine formulae for the π 's, 5 variables are selected as references and then are combined with each of the remaining 4 variables. Solving constructs such as

$$\pi_1 = h^a g^b k^c \mu^d \alpha^e C_p \quad (2)$$

where a to e are integers, provides the classical π groups (Table 2, left). Although dimensional analysis reveals the π groups, it does not describe how to combine the π 's into relevant, dimensionless

Table 1 Variables and unit-dimensions relevant to convection in the laboratory and planets

Variable	Symbol	Units‡
Classical (constant P)		
Length scale	h	L
Gravitational acceleration	g	L/t^2
Temperature difference	ΔT	T
Heat transfer coefficient	H	$Q/(L^2 t T)$
Fluid density*	ρ	M/L^3
Volumetric expansivity*	α	$1/T$
Heat capacity*	C_p	$Q/(MT)$
Thermal conductivity*†	k	$Q/(L t T)$
Viscosity*†	μ	$M/(L t)$
Additions for planets		
Pressure difference	ΔP	P
Compressibility*	β	$1/P$
Outer radius§	R_{out}	L
Shear modulus (elastic)*§	G	P
Yield stress (plastic)*§	σ_{yield}	P
Effective deviatoric stress*§	$\delta\sigma$	P
Mass diffusion*§	D_m	L^2/t
Grain size*§	d	L

*Designates a material property of the fluid or medium. †. Thermal diffusivity (of phonons) κ and kinematic viscosity are used instead of thermal conductivity and dynamic viscosity in the Ra and Gr numbers, due to cancellations. §. Denotes variables important to planets, but not previously incorporated in dimensional analysis, see text. ‡. L=length, t=time, T=temperature, Q=energy, M=mass, P=pressure (provision of units does not link the variables.). In mathematical descriptions of free convection, energy is relevant but not velocity (which is fundamental for forced convection and enters into the Reynolds number). This stems from the Grashof number occurring as a parameter inside flow equations which do contain velocity terms. Like energy, P is a dimension in planetary convection, due to this being an independent thermodynamic parameter arising from gravitational forces. Force, area, and volume enter into stability analysis via physical constraints, see the text.

Table 2 Dimensionless groups and numbers used analyzing natural convection

Classical group	Classical number	Planetary group	Planetary number
$\pi_1 = \frac{\mu C_p}{k} = \frac{\nu}{\kappa}$	= Pr*	$\pi_5 = \beta \Delta P = \frac{\Delta P}{B_T}$	in the adiabat
$\pi_2 = \alpha \Delta T$	in Gr, Ra	$\pi_{6,\text{sphere}} = \left(1 - \frac{h}{R_{\text{out}}}\right)^2$	in Gr, Ra, Nu
$\pi_3 = \frac{h^3 g \rho^2}{\mu^2} = \frac{h^3 g}{\nu^2}$	in Gr, Ra	$\pi_7 = \frac{\delta \sigma}{\sigma_{\text{yield}}}$	see text
$\pi_4 = \frac{Hh}{k}$	= Nu*	$\pi_8 = \frac{\kappa}{D_m}$	= Le*†

Notes: Laboratory settings explored classically (left) are compared to additional groups needed to address interiors of planets (right). Classical groups have been calculated by choosing h , g , k , μ , and α as references, in which case C_p , ΔT , ρ , and H are additional variables, see text. Variables are defined in Table 1. Planetary π 's are numbered in order of appearance in the text. Previous analyses of planets and atmospheres incorporate π_5 into Gr and Ra via the adiabat (see text). Three additional groups are proposed for planets: π_6 , which provides for mass conservation in spherical geometry; π_7 , which describes onset of flow in an ideal Bingham plastic, and π_8 which describes the competition of thermal and mass diffusion. *. Lattice heat transport is assumed. Radiative transfer is an additional mechanism that can be important for transient heat flow at high T (Hofmeister, 2010), which will increase κ (and k) but are unimportant to slow cooling. Grain size does not enter into our models. †. $\text{Sc} = \nu/D_m = \text{LePr} = \pi_8 \pi_1$ is redundant: Le is germane because it compares the two diffusivities, see text.

numbers. Dimensionless numbers are fewer in number than the π 's because additional constraints, such as conservation laws or force balance, are invoked when deriving them. Regarding natural convection, two π groups reproduce the Prandtl (Pr) and Nusselt (Nu) numbers, whereas π_2 times π_3 forms the Grashof number (Gr), and Ra follows (Table 2, left). Because $\text{Ra} = \text{GrPr}$, only 3 dimensionless numbers are needed to describe free convection classically. Additionally, other types of dimensional analysis can be performed (e.g., Bridgeman, 1927). A common approach is to simplify the equations using the unit dimensions of the parameters which then allows estimation of results. The approach in geodynamics has been to modify the existing dimensionless numbers. Two modifications are currently used, as follows.

1.2 Is Pressure Adequately Addressed in Current Modifications to Ra?

Existing discussions of planets incorporate two more variables, ΔP and B_T , and one new unit-dimension, creating π_5 . The importance of pressure relative to temperature is estimated from their relative effects on volume

$$\frac{\pi_2}{\pi_5} = \frac{\alpha_V \Delta T}{\beta \Delta P} = \frac{\alpha_V \Delta T}{B_T^{-1} \Delta P} \quad (3)$$

Typically, α_V is $\sim 3 \times 10^{-5}/\text{K}$. For the whole mantle, $\Delta T \sim 4000$ K is suggested from melting of Fe-S in the core (Chudinovskikh and Boehler, 2007); seismology gives $\Delta P = 135$ GPa and average $B_S \sim 360$ GPa (e.g., PREM: Dziewonski and Anderson, 1981). Across the upper mantle (UM) and transition zone (TZ), ΔT is smaller, ~ 2000 K (Agee, 1998), $\Delta P = 24$ GPa, and average $B_S \sim 170$ GPa (PREM). Hence, π_2/π_5 is ~ 0.32 for whole mantle and ~ 0.64 for upper mantle.

Small π_2/π_5 indicates that pressure is more important than temperature to Earth's interior, which is consistent with seismologic observations of density increasing downward, despite temperatures climbing. Moreover, as is well documented by research in mineral physics, pressure dominates behavior inside

Earth's mantle, inducing phase transformations, increasing coordination numbers of most elements (including Si), and causing close-packing of O-atoms (Prewitt and Downs, 1998). Therefore, a significant correction of Ra which addresses the impact of pressure upon solid material properties is expected. The existing correction considers the effect of pressure on the temperature difference and buoyancy. Because elastic compression is instantaneous compared to thermal diffusion, $B_T^{-1} \Delta P$ does not alter buoyancy computed from density differences. Instead, this factor enters into the adiabatic correction of $\Delta T^* = \Delta T(1 - \gamma_{\text{th}} B_T^{-1} \Delta P)$, which is based on behavior of the atmosphere. Specifically, ΔT is reduced in accord with an adiabatic gradient (Tritton, 1977)

$$\left. \frac{\partial T}{\partial P} \right|_S = \frac{\gamma_{\text{th}} T}{B_S} \quad (4)$$

where $\gamma_{\text{th}} = \alpha B_S / \rho C_p = \alpha B_T / \rho C_V$ is the thermal Grüneisen parameter, and B_T is the isothermal thermal bulk modulus, which is the inverse of compressibility, $\beta = V^{-1} \partial V / \partial P|_T$. Because $B_S = B_T(1 - \alpha_V \gamma_{\text{th}} T)$ is only $\sim 3\%$ larger, either modulus is suitable, and likewise for heat capacity (C), leading to reduction of ΔT for Earth's mantle by only $\sim 30\%$, which is insignificant compared to the excess of Ra over critical. This minor change is insufficient given the role pressure plays in determining the state of a material.

Importantly, Eq. (4) describes an isentrope (the subscript S denotes constant entropy), not an adiabat. Adiabats (no heat exchange) are considered to be equal to isentropes when reversibility applies (e.g., Fegley, 2015). The equivalence of adiabats and isentropes for the ideal gas can be obtained from its heat capacity and equation of state (e.g., Fegley, 2015), and thus Eq. (4) is a reasonable approximation for the atmosphere. The Earth, in contrast, is not a gas and changes in the evolving Earth are irreversible, as is the case for natural or spontaneous processes (Zemansky and Dittman, 1981). Non-adiabatic conditions (internal heating) are discussed below.

Equations of state for solids are unlike those of gas. Behaviors associated with solids are unlike those for fluids. Hence, other properties of solids, all with dimensions of pressure (Table 1), should be considered in the dimensional analysis of Ra for a planet. This requires more π 's, which affects the dimensionless numbers (Table 2). Because the maximum pressure is dictated by the mass and outer radius of the planet, Section 2 considers the radius in detail, which is also the main geometric constraint.

1.3 Is Internal Heating Correctly Addressed in Current Modifications to Ra?

Formulae in geodynamics addressing internal heating provide a stronger dependence on depth than the classical Ra (e.g., Schubert et al., 2001). The stronger dependence is obviously in error because internal heating warms the center of the box, rather than the bottom (e.g., Carslaw and Jaeger, 1959) thereby increasing the stability of the bottom half.

We quantify the effect of internal heating on the temperature gradient by considering solutions for a slab (flat box) with constant properties k and κ and internal heat production of A_0 (= Watts per volume). In order to sum (superimpose) solutions to the heat equation for the cases of basal and internal heating, T of both surfaces for the internal heating case are held at 0°C and the vertical direction is defined as extending from $-L$ to $+L$ (Fig. 1, top row). This geometrical constraint means that h in

the Ra number is related to $2L$ of the conductive problem. From Carslaw and Jaeger (1959), the solution as a function of time is

$$T = \frac{A_0 L^2}{2k} \left[1 - \frac{z^2}{L^2} - \frac{32}{\pi^3} \sum_{n=0}^{\infty} \frac{(-1)^n}{(2n+1)^3} \cos \frac{(2n+1)\pi z}{2L} \exp \left(\frac{-\kappa(2n+1)^2 \pi^2 t}{4L^2} \right) \right] \quad (5)$$

After a very long time, the temperature in the middle of the slab ($z=0$) approaches the steady-state solution of $T_{\infty,0} = A_0 L^2 / (2k) = A_0 h^2 / (8k)$. At any time, the maximum temperature is at the center of the slab. For illustrative purposes, we consider linear temperature gradients from the middle to the surfaces (Fig. 1a), which suffice, due to the slow heating quantified below and to the assumption of constant κ .

Although the dependence of $T_{\infty,0}$ on h is strong, A_0 is very small for the Earth, being equivalent to ~ 100 W per km^3 , or one candle to heat a major city (e.g., van Schmus, 1995). Thermal diffusivity of ~ 1 $\text{mm}^2 \cdot \text{s}^{-1}$ and thermal conductivity of ~ 3 $\text{W} \cdot \text{m}^{-1} \cdot \text{K}^{-1}$ are typical values in mantle models (e.g., Davies, 2011). With weak heating and inefficient conduction, ~ 100 Ga is required to reach steady-state inside an immense slab (Fig. 1e). That steady-state conditions do not describe Earth's mantle was demonstrated using exact and approximate solutions for

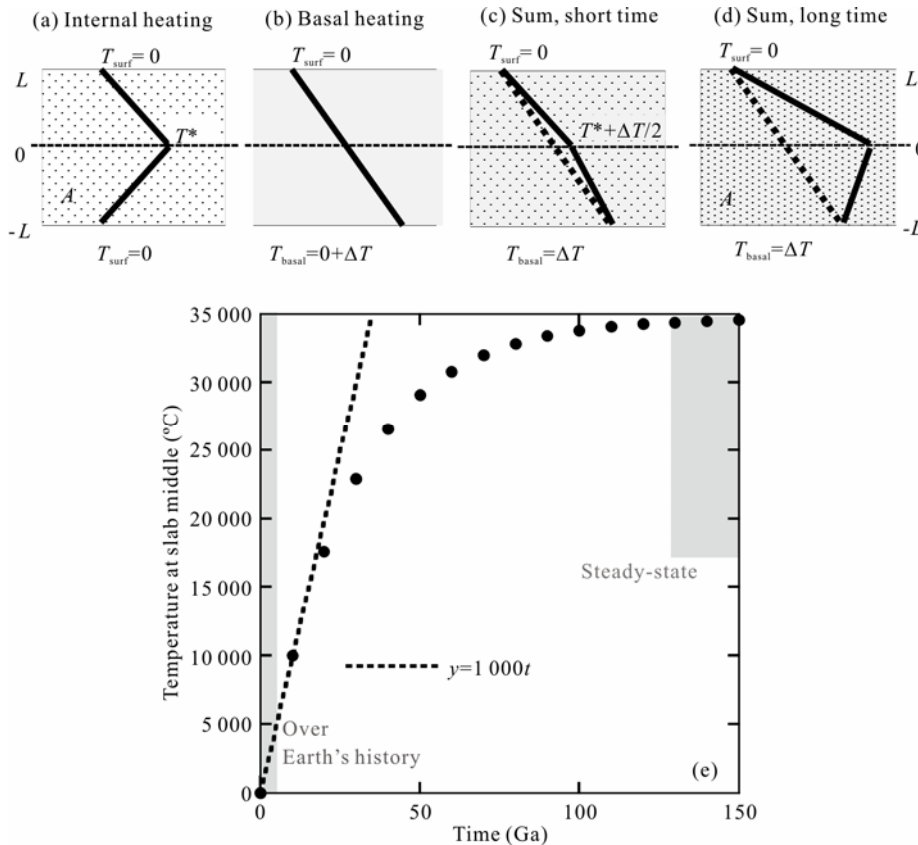


Figure 1. Temperatures in the infinite slab for internal and basal heating. Top, geometry and conditions in the slab with vertical size $h=2L$. (a) Solving for $T(t,z)$ with internal heating requires setting $z=0$ in the middle of the slab. T^* is the temperature achieved after some time t . (b) For basal heating, the T gradient is imposed and is independent of time. (c) Summation of basal and internal heating for short time, when $T^* < T_{\text{basal}}$. (d) Summation of basal and internal heating when $T^* > T_{\text{basal}}$, which requires a long time to develop. In both cases, internal heating stabilizes the bottom half of the slab against convection. (e) Dependence of T^* on time for thermal properties appropriate to the mantle (see text). Grey bars indicate relevant time scales.

the sphere (Criss and Hofmeister, 2016). Over 4.5 Ga, only the outer 670 km of the Earth would have cooled conductively. The immensity of $\sim 35\,000$ K for $T_{\infty,0}$ further emphasizes that the steady-state approximation is inappropriate for the Earth.

Previous analyses (e.g., Schubert et al., 2001), amend the Ra based on the steady-state solution to an internally heated slab. Furthermore, these works substitute L for h in the Ra, and thereby ignore the fact that an internally heated slab is warmest in the middle. A hot middle (long term solution) makes it impossible for lower half of the slab to convect (Fig. 1d). Short times are relevant (Fig. 1c). For this case, internal heating destabilizes the upper half of the slab, at the expense of stabilizing the lower half. Because the internal heating of the Earth is weak, this destabilizing effect should be neglected, especially insofar as ΔT is an estimate. We return to the issue of internal heating in Section 3.6.

1.4 The Need for Further Modifications to the Planetary Ra

From Sections 1.2 and 1.3, treatment of heat transfer in the current adaptations of Eq. (1) to planets is problematic. Additional factors of obvious importance to Earth's interior warrant discussion. In particular, solids behave differently than liquids in fundamental ways. Liquids flow under any stress. In contrast, solids resist deformation. The response of a solid is elastic at low stress, but plastic at high stress. Plasticity is not equivalent to viscous flow (Hill, 1950). Based on deformation measurements, Hiraga et al. (2010) concluded that the perpetual, fluid-like behavior underlying mantle convection models is unattainable due to micromechanical changes which always accompany the deformation of solids. See Section 3.4 for further discussion.

Another crucial difference is that in gases and liquids, molecular motions carry both heat and mass, thereby providing similar diffusivities; whereas in solids, the flow of heat is fully independent of flow of mass, providing vastly different thermal and mass diffusivities (tabulated in Sec. 3 with additional discussion). Existence of an independent mechanism for heat flow in solids permits large temperature gradients to exist across non-convecting solids up until melting temperatures are reached. This behavior is exemplified by conditions in the oceanic lithosphere, which is melted at its base. Yet, this key behavior is not addressed in the classical Ra. Interestingly, the high Prandtl number ($Pr = \nu/\kappa$) of the mantle indicates that heat transfer is independent of inertial effects (e.g., Elder, 1976) but the effect of this known decoupling on the Ra has not been theoretically explored. Experimentally, convective flow has only been observed in relatively inviscid materials ($\nu \sim 22\,000$ mm²·s⁻¹ as in syrup: White, 1988). Yet, this 17 orders-of-magnitude extrapolation has not been questioned when using Ra to describe Earth's mantle.

From the above, the classical formulation for Ra seems inappropriate not only for the solid state, but moreover for the high internal pressure provided by self-gravitation of planets. Additional issues are explored below, beginning with the special nature of spherically symmetric geometry.

2 MASS CONSERVATION DURING FLOW IN RADIAL SYMMETRY

The classical derivation of the Rayleigh number considers

bottom heated convection occurring in Cartesian coordinates. Clearly, this model differs significantly from the conditions inside planets and stars. This section will demonstrate that modeling cylindrical or spherical symmetry using Cartesian coordinates grossly violates mass conservation. Violations of mass conservation even over small scales have consequences for mantle convection models (Hetényi, 2014).

Classically, vertical instability is considered, which is analogous to radial instability in planets. Solely angular motions in planets are related to spin and are not driven by buoyancy differences. Because volume elements in Cartesian, cylindrical, and spherical-polar coordinate systems have different shapes, rules for mass conservation during motions of these elements will differ among these three systems, as follows.

Under constant P and T , equal thickness (δh) layers in a box have the same mass whereas mass in concentric shells of equal thickness (δr) in a sphere differs because shell area varies with radius (Fig. 2). For spherical geometry, length scales require amending to conserve mass during its transfer between shell-shaped layers

$$L = h \frac{R_{in}^2}{R_{out}^2} = h \frac{(R_{out} - h)^2}{R_{out}^2} = h \left(1 - \frac{h}{R_{out}}\right)^2 = h\pi_6 \quad (6)$$

Conserving momentum and heat during flow requires the same scaling (Fig. 2). Thus, for planets, which are nearly spherically, both Ra and Gr must be multiplied by π_6^3 and Nu by π_6 .

Note that π_6 accounts for planetary geometry differing from parallel plates, without involving any other parameter. As a consequence, the effects of physical properties are independent of geometry and can be evaluated by considering vertical instability in a Cartesian reference frame.

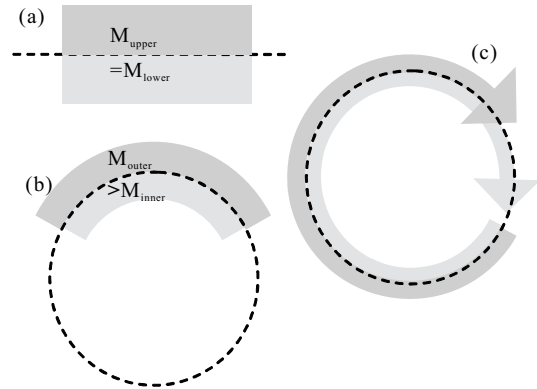


Figure 2. Schematics in 2-dimensions illustrating how geometry affects scale length in dimensional analysis. (a) Mass balance of parallel layers with equal thickness and density in Cartesian geometry. (b) Imbalanced mass in concentric layers with equal thickness and density. Note that if heat energy is considered in terms of heat density (energy per volume), then for equal thickness layers, the same imbalance occurs as for mass. (c) Viscous motion in concentric shells. At the same tangential velocity, motion in the inner circuit completes the circle, whereas the outer circuit falls short. For a laminar momentum balance with no shear, the outer layer must be thinner (less mass) which makes it faster, and hence a correction factor is needed for the length scale describing flow. Equation 6 gives the correction factor (π_6) for spherical coordinates. For cylindrical symmetry, $\pi_6 = (1 - h/R_{out})$.

3 EVALUATION OF VERTICAL INSTABILITY

This section begins by considering the physical implications of Gr and Ra for pourable fluids in a box. Then we adapt these classical formulations to address the defining properties of solids.

3.1 Derivation and Meaning of the Grashof Number

Because energy barriers are nearly negligible for positional rearrangements in liquids, this state flows under any stress (Fig. 3). The Grashof number (Gr) describes whether a fluid is vertically unstable

$$\text{Gr} \equiv \frac{F_{\text{buoyancy}}}{F_{\text{drag}}} = \frac{\alpha_v \Delta T g h^3}{\nu^2} \quad (7)$$

To derive Gr, we presume that shear stresses (σ_{shear}) in liquids arise from drag during viscous flow, after Newton

$$\sigma_{\text{shear}} \equiv \nu \rho \frac{\partial u}{\partial y} = \frac{F_{\text{drag}}}{A} \quad (8)$$

where A is area, u is speed, and y is the horizontal direction. Rearranging and applying dimensional analysis

$$\nu = \frac{\partial y}{\partial t} \frac{m(\partial u / \partial t)}{A(m / Ah)} = \frac{h}{u} \frac{u}{t} h = \frac{h}{t} h = u_{\text{flow}} h \quad (9)$$

where t is time. Incorporating the adiabat into the buoyancy force, ratioing this against F_{drag} of Eq. (8), and utilizing Eq. (9) gives for the pourable, liquid state

$$\begin{aligned} \frac{F_{\text{buoyancy}}}{F_{\text{drag}}} &= \frac{\rho_0 \alpha_v \Delta T^* g h A}{A \rho_0 \nu (\partial u_{\text{flow}} / \partial y)} = \frac{\alpha_v \Delta T^* g h}{\nu (u_{\text{flow}} / h)} \\ &= \frac{\alpha_v \Delta T^* g h^3}{\nu (u_{\text{flow}} h)} = \frac{\alpha_v \Delta T^* g h^3}{\nu^2} = \text{Gr} \end{aligned} \quad (10)$$

3.2 How Deformation of Solids Differs Significantly from Flow of Liquids

Understanding the response of solids to stress is an important component of several fields, especially mechanical engineering and solid mechanics, where both realistic and ideal behaviors have been explored in detail. The theoretical basis was established in the mid-1800s, predominantly by Cauchy (Soutas-Little, 2011). Development of solid mechanics is ongoing, motivated by the need to predict the failure of increasing complex structures, as well as by the quest to understand the complex behaviors of real world materials.

Actual properties of materials and structures often vary considerably from their theoretical values. For instance, the actual failure strength of materials is approximately 50× to 500× lower than the theoretical value, a function of imperfect structure and impurities. An extreme example of this are welded structures, where the properties are dependent on both the new alloy created, and the flaws introduced by the welding process (Criss et al., 2015).

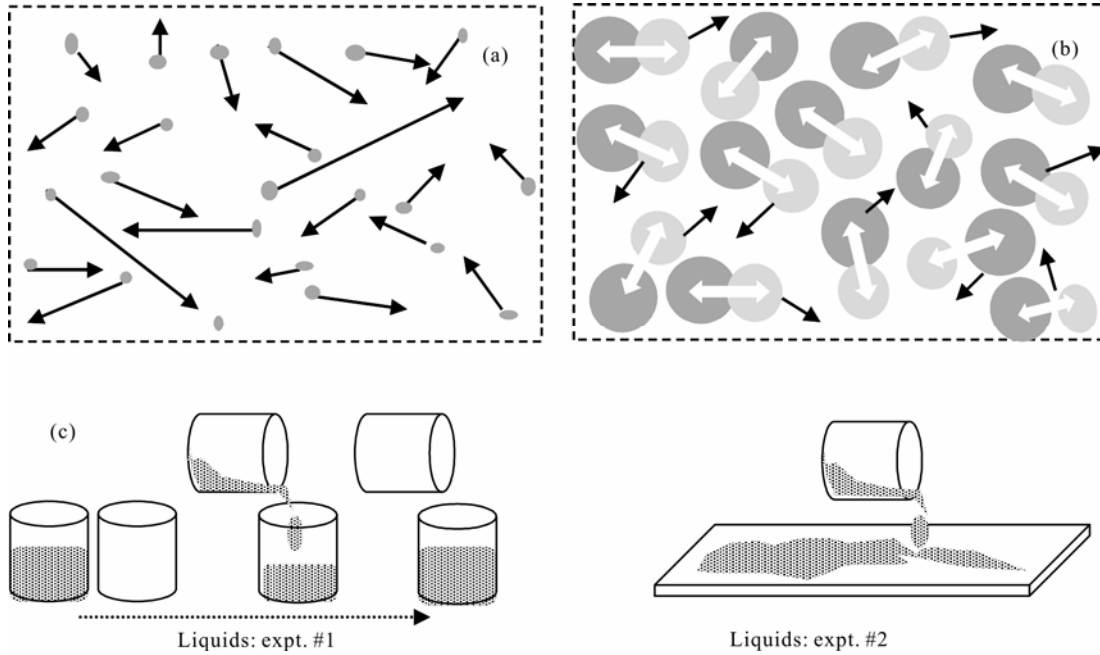


Figure 3. Schematics of mechanisms for fluids. Grey circles=atoms; black arrows=direction of translational motions; white arrows=vibrations of atomic bonds. (a) Monatomic gas, where interactions are limited to brief collisions and exchange of energy is entirely kinetic. Motions occur even in the absence of organized flow. (b) Pourable liquid, where translational motions are somewhat impeded by neighboring molecules. Energy exchanges are mostly kinetic but vibrational energy can be exchanged between molecules during collisions. As density and molecular size and complexity increase, motions become more hampered and vibrations become increasingly important to the transfer of energy. (c) Reaction of liquids to stress. In experiment #1, the liquid can be poured from beaker to beaker with turbulent mixing, yet the material properties remain unchanged even though the internal arrangement of the constituent molecules has greatly changed. Experiment #1 can be repeated indefinitely. In experiment #2, pouring the liquid into a puddle drastically changes its shape and entirely rearranges the molecules, but the physical properties are not changed, so long as the puddle is at least a few molecules thick. In both experiments, negligible deviatoric stresses exist after motion ceases, despite large strains and distortions.

Studies of the deformation of Earth materials began in the 1950s with the pioneering work of Griggs. Although this later research uses already developed precepts from materials science, the underlying physics has not been entirely adhered to. In part, this is because conditions in the lower mantle are simply not attainable in the laboratory. This section summarizes what is known from materials science and engineering and where this diverges from mantle extrapolations.

Mantle solids are characterized by 3-dimensional linkages of strong ionic bonds (Fig. 4). Multiple types of plasticity are observed in candidate materials, including motion of dislocations, atomic diffusion, and dynamic recrystallization (Kohlstedt and Hansen, 2015). These sluggish mechanisms require substantial energy to break and reform atomic bonds.

Breaking all bonds in a solid, which permits rearrangement analogous to liquid motion, is described by Frenkel's (1926) theoretical shear stress, which is generally many times the actual ultimate stress. Furthermore, once broken, it is necessary to reform all of these bonds. Hence, viscous flow is possible in solids, but is limited to certain materials above the glass transition. In contrast, a different process, known as creep, typically occurs in metals and ceramics when the temperature exceeds 50% of melting (Meyers and Chawla, 2009). That certain mathematical descriptions of creep (e.g., Nabarro-Herring or Coble) can be recast to mimic forms of equations

that depict Newtonian viscous behavior (e.g., Kohlstedt and Hansen, 2015) has supported modeling the solid mantle as if it were fluid. This approximation is over-simplified for the following reasons.

(1) The equations of Nabarro-Herring (for high T lattice diffusion) or Coble (for lower T grain boundary diffusion) referred to in Earth science studies incompletely describe creep. The more general Mukherjee-Bird-Dorn equation (Mukherjee et al., 1969) expresses the rate of creep ($\dot{\epsilon}$) in terms of stress, temperature, Burgers vector (b), and grain-size (d)

$$\frac{\partial \epsilon}{\partial t} = \frac{BGb}{kT} D_0 \exp^{-Q/RT} \left(\frac{b}{d}\right)^p \left(\frac{\sigma}{G}\right)^n = B^* \exp^{-Q/RT} \quad (11)$$

where G is the shear modulus, k is Boltzmann's constant, R is the gas constant, Q is an activation energy, and D_0 , B^* , B , p , and n are various parameters depending on the material. Diverse materials may be described by Eq. (11) so long as they experience steady state creep, and have a grain size (Meyers and Chawla, 2009). The important exponential factor (n), which describes a key difference between creep and viscous Newtonian flow (Mukherjee et al., 1969) is missing from the Nabarro-Herring formulation which restricts two free parameters, namely, $p=2$ and $n=1$. Both Eq. (11) and the general, nonlinear stress-strain rate equation describing superplasticity ($\sigma = K\dot{\epsilon}^m$) have forms unlike that

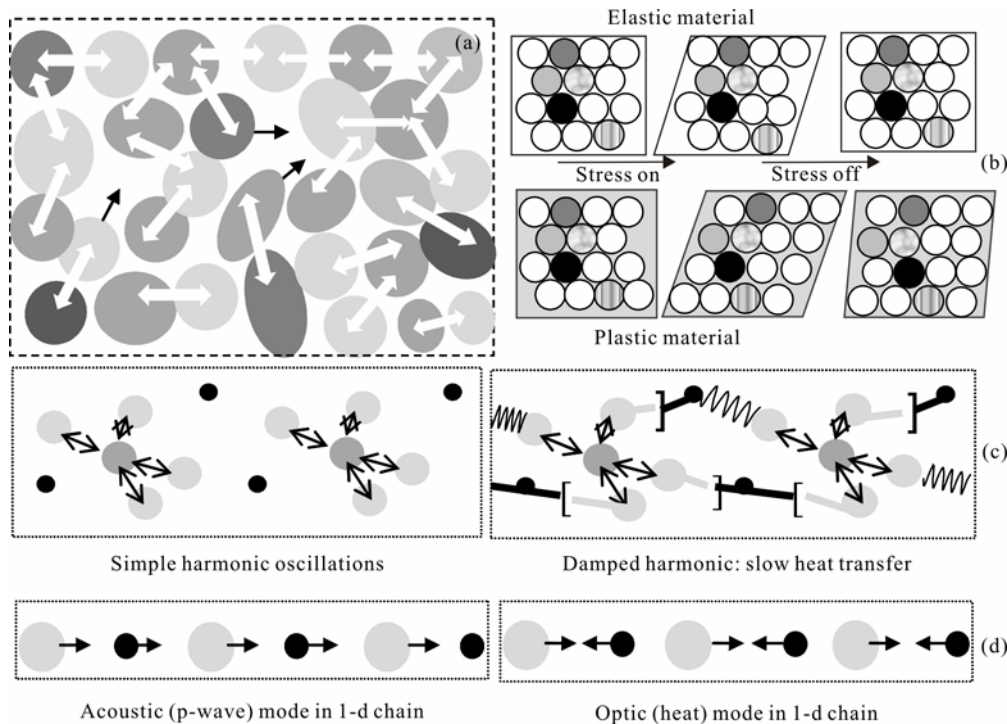


Figure 4. Schematics of micromechanical mechanisms for ionic and metallic solids. Symbols as in Fig. 3. (a) Solid that is not stressed. Interatomic bonds link constituent atoms in all directions; vibrations are similarly linked. Atoms can diffuse where defects exist, as suggested by the “holes” and black arrows. (b) Comparison of reversible deformation of an elastic solid (top row) to irreversible deformation of a plastic solid (bottom row). As indicated by the “marked” atoms, the elastic solid returns to the same internal configuration and macroscopic shape after the applied stress is removed. After some substantial stress is applied to a plastic solid, internal rearrangements exist: thus, upon removal of the stress, the material can neither return to its original shape nor internal configuration. (c) Relationship of vibrational modes to heat transfer and attenuation in an elastic solid. Left, unachievable perfect harmonic oscillations once set in motion, continue indefinitely, and are not attenuated. Right, in a solid, vibration of one bond is influenced by motion of neighbors, which creates damping. Heat transfer is finite and slow. (d) Acoustic modes involve atoms moving together (left diagram of the 1-d chain) whereas optic modes involve motions in opposition (right) which makes heat transfer much more strongly attenuated than is sound.

describing a Newtonian fluid (e.g., Meyers and Chawla, 2009).

(2) Grain-size is important to creep and enters into many descriptions of the deformation of solids, including Eq. (11), but is irrelevant to liquids and Ra.

(3) Formulations for steady-state (stage II) plasticity considered above are invalid in other regimes: elastic behavior, strain hardening, necking, or failure (Figs. 4–7). The behaviors illustrated are schematic: regarding the mantle one should envision different grains being stretched and thinned during flow. The possibility of superplasticity, whereby creep extends to higher stress and strain than “expected,” has been called on to justify application of fluid dynamics to solids. However, superplastic solids also harden and fail (Mitchell, 2004). Four different modes of failure have been documented (Langdon, 1982). Hence, the inferred perpetual fluid-like behavior assumed in mantle convection models is unexpected. In analyzing deformation of silicate material, Hiraga et al. (2010) recognized and noted that this is a serious flaw in mantle convection models. Although the experimental component of this paper is well-cited, the importance of Hiraga et al. (2010) deduction has been overlooked. We attribute the latter to widespread belief that the classical Ra number is valid for solids.

(4) Most importantly, an elastically or plastically deforming solid is under nearly perfect force balance, even if the applied forces are high, because the accelerations are extremely low. In particular, solids undergoing primary (stage I) plasticity decelerate into steady-state creep which occurs at the minimum creep rate (e.g., Meyers and Chawla, 2009). Lattice deformation forces providing this behavior are not accounted for in Gr or Ra which instead describe the flow of liquid, which arises under any amount of stress.

3.3 Stability Criteria for an Ideal, Bingham Plastic

To better account for behavior inherent to solids (Fig. 5) in accessing stability, we consider the idealized behavior of a Bingham plastic (Fig. 6), which is simple, yet includes both

elastic (solid) and viscous (liquid) regimes. Differential stress is considered. Although deviatoric stress provides a more complete representation, it is not directly measured in experiments. Bingham’s model, which requires a minimum shear stress (σ_{yield}) for plasticity, has been applied to muds, glasses, and other geologic materials with both liquid and solid components (Sehlke et al., 2014; Davis and Selvadurai, 2005). Similarly, mantle materials require significant differential stress to deform (Figs. 5–8). Generalizing these observations indicates that a minimum effective deviatoric stress ($\delta\sigma = \sigma_{\text{yield}}$) is required for solids to enter a regime of liquid-like behavior: once a solid enters this regime, Gr and Ra become relevant. This observation constitutes a π -group

$$\pi_7 = \frac{\delta\sigma}{\sigma_{\text{yield}} > 1} \quad (12)$$

Below σ_{yield} , conditions are elastic whereby solids respond to temperature, hydrostatic compression, and shear stress as described respectively by α , bulk (B) and shear (G) moduli

$$G \equiv \frac{\text{shear stress}}{\text{shear strain}} = \frac{\delta\text{force} / A}{\delta h / h} \quad (13)$$

Convection is unexpected for $\pi_7 < 1$.

3.4 How Diffusion in Solids Differs from Diffusion in Liquids

Heat transport for constant thermal diffusivity κ is governed by

$$\frac{\partial T}{\partial t} = \kappa \frac{\partial^2 T}{\partial z^2} \quad (14)$$

where z is the vertical direction. Dimensional analysis (e.g., Hofmeister, 2010) relates κ to mean free path (λ), mean free lifetime (τ), and the velocity of the particle carrying the heat (u_{micro}).

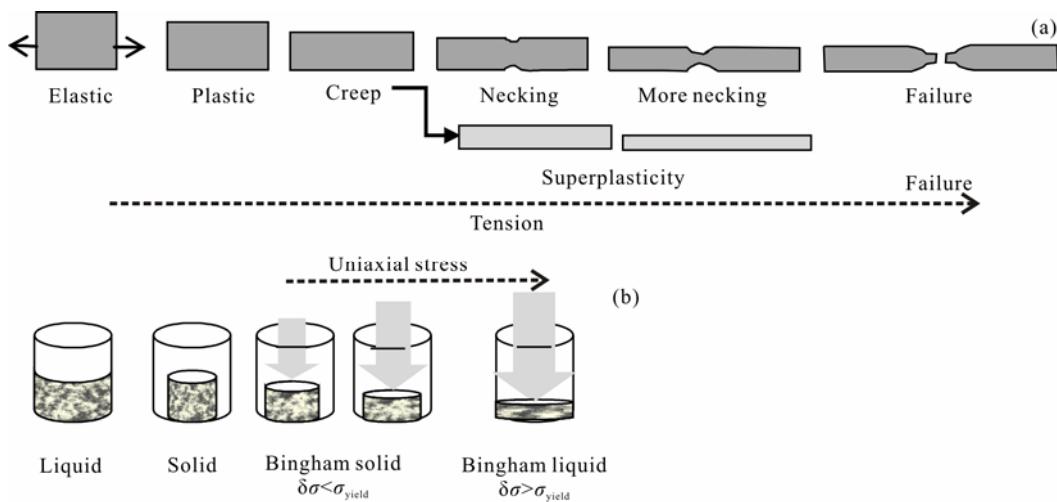


Figure 5. Schematics of mechanical response to stress. (a) Time-progression of object shape for a plastic solid undergoing creep in tension, which is the condition used to establish superplasticity (see Hiraga et al., 2010). At high stress, the onset of failure is usually marked by necking. Failure occurs before the area of the neck disappears. During superplastic behavior, necking may be postponed, but failure still occurs at some high stress. In contrast, liquids thin evenly, and remain coherent until only a few molecules thick. (b) Comparison of a liquid, which flows under any stress and requires a container for shape, to behavior of a Bingham plastic, which has a shape and cannot flow unless stress is high.

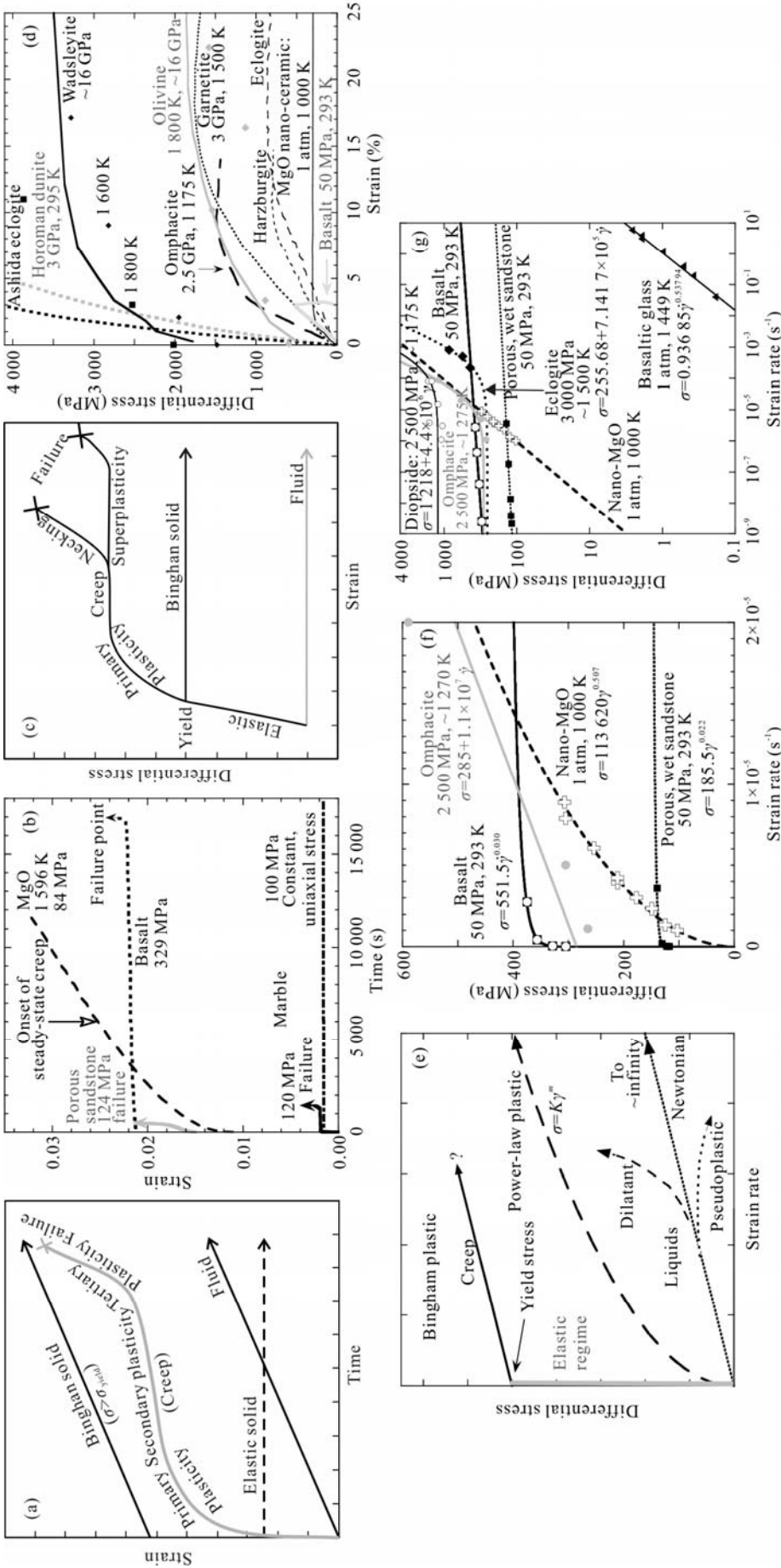


Figure 6. Rheologic behavior, emphasizing differences between liquids and solids. Panels (a), (c), and (e) illustrate theoretical behavior using true differential stresses and true axial strains. Fluids flow under any deviatoric stress. A Bingham plastic will also flow, but only above the yield (shear) stress. Typical plastics exhibit hardening behavior during primary plasticity. Under certain conditions, plastics can deform without hardening, called creep. Failure follows. Panels (b), (d), and (f) show typical data for rocks and ceramics corresponding to panels (a), (c), and (e), respectively. Engineering stress and engineering strain $= (L_p - L_0)/L_0$ are presented, because these were specified in most studies, and differ little from true stress or strain at the low strains measured. Net confining pressure, P_{confin} , is reported, which is lower than the hydrostatic pressure $P_{hydro} = P_{confin} + \frac{1}{3}(\sigma - \sigma)$ under uniaxial compression. Further details: (b) Time evolution. For each experiment, the average, nearly constant stress is listed. Permeable Etina basalt with ~4% porosity and ~mm phenocrysts in a fine-grained matrix at ~293 K, 50 MPa confining pressure and 20 MPa pressure of internally induced fluid from Heap (2009) and Heap et al. (2011). Tennessee marble with ~mm grain-size at ~293 K and ~0 confining pressure from Costin (1985). MgO ceramic, with ~4% pores and 0.012 mm grain-size, at 1.596 K and ~0 confining pressure with elastic strain subtracted from Birch and Wilshire (1974). (d) Stress vs. strain data. Heavy dotted lines=dunite with 0.5% porosity at 3 GPa confining pressure and 295 K and a similar eclogite from Shimada et al. (1983). Fine patterned lines=true strain data on eclogite, garnetite, and harzburgite all harzburgite of ~0.04 mm grain-size at 1.500 K and 3 GPa confining pressure (Jin et al., 2001). Solid line=nano-crystalline MgO (spark fused to remove pores) at 1.000 K and no confining pressure (Dominguez-Rodriguez et al., 2007). Symbols and heavy solid lines=X-ray data and fits for wadsleyite at two temperatures and olivine (Nishihara et al., 2008). Omphacite (75% jadeite-25% diopside) from Moghadam et al. (2010). (f) Stress vs. strain rate data on a linear scale whereas (g) is a log-log scale with power-law and linear fits. For both parts: Etina basalt and Daryl Dale sandstone both at 293 K, 50 MPa confining pressure with 20 MPa pressure of internally induced water from conventional experiments of Heap et al. (2011) and Heap (2009). Synthetic omphacite and diopside at 2.500 MPa and 900 to 1.000 °C from Moghadam et al. (2010). Synthetic eclogite of ~0.04 mm grain-size at 1.500 K and 3 GPa confining pressure (Jin et al., 2001). Nano-crystalline MgO (spark fused to remove pores) at 1.000 K and no confining pressure (Dominguez-Rodriguez et al., 2007). Glass with ~33% crystals, made from Hawaii basalt, and measured in a concentric cylinder viscometer at 1.176 K and no confining pressure (Sehlik et al., 2014). The yield strength is ~8.2 Pa and increases with crystal fraction, whereas crystal-free glasses exhibit Newtonian (fluid) behavior.

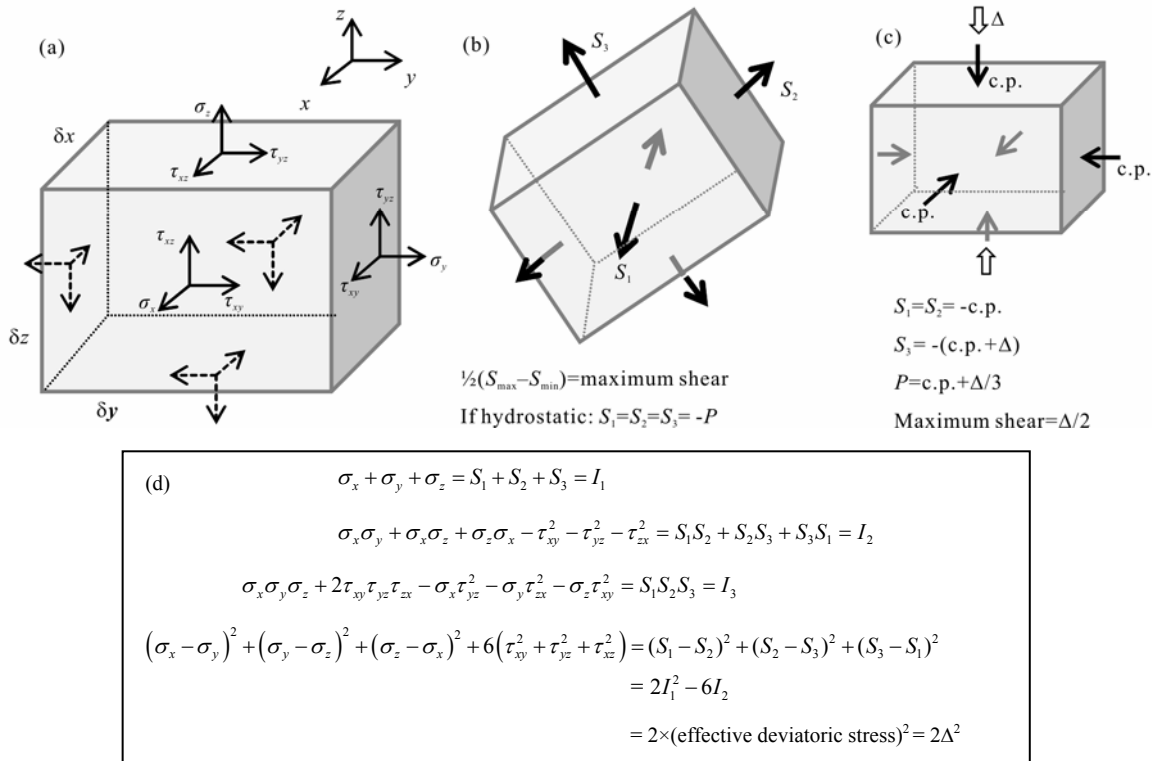


Figure 7. Schematic showing infinitesimal stress elements, common experimental conditions, and governing equations (after Timoshenko and Goodier, 1970). (a) Stress elements under a generic stress, showing the orientation of all normal and shear stresses. (b) Orientation corresponding to a diagonalized stress matrix. In this orientation, the shear stresses disappear, and the normal stresses are the principal stresses (S_1, S_2 , and S_3). Equations below the tilted element provide the maximum shears and the special conditions of a hydrostatic environment. (c) Laboratory conditions of confining and differential stresses. The addition of an additional differential stress increases the hydrostatic stress, and induces shear stresses in the sample. (d) Equations for the three primary stress invariants (I_1, I_2, I_3) and one additional deviatoric invariant which remain constant despite rotation of the stress element. The final invariant (Δ) is directly involved in the von Mises yield criterion, and is referred to as the effective deviatoric stress ($\delta\sigma$).

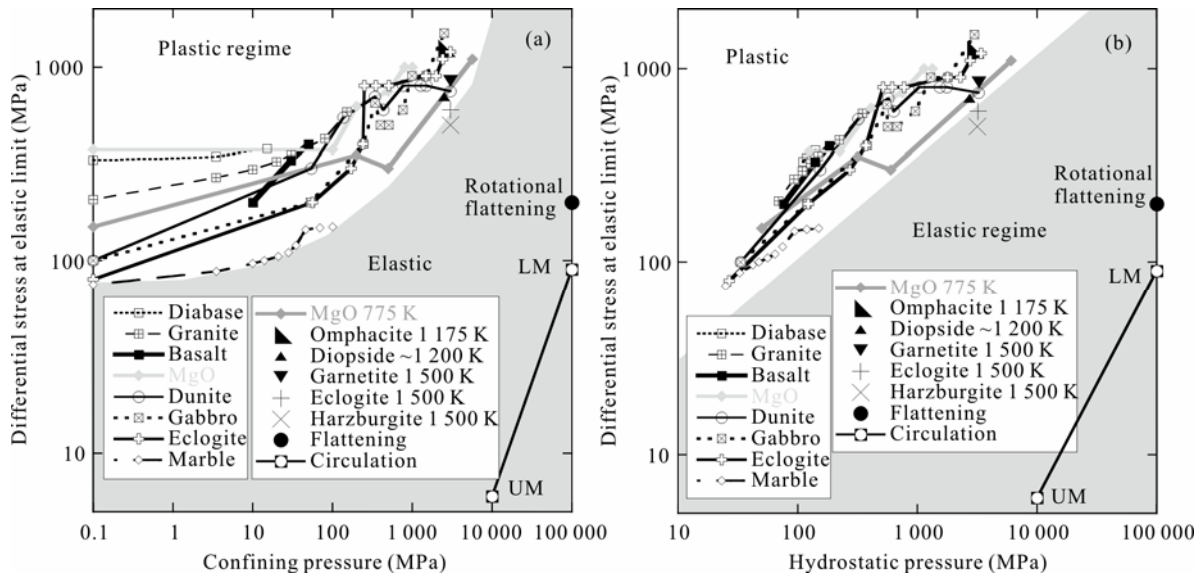


Figure 8. Comparison of the elastic limit for differential stress from experiments to mantle conditions. (a) Confining pressure. (b) Hydrostatic pressure. For both panels, room temperature data are listed in the left inset: dunite, gabbro and eclogite from Shimada et al. (1983). Basalt from Heap et al. (2011). Diabase and granite from Wawersik and Brace (1970). Marble from Paterson (1958; see Heep, 2009). MgO from Paterson and Weaver (1970). High temperature data listed in the right inset: MgO with no confining pressure from Domínguez-Rodríguez et al., 2007, at moderate pressure from Paterson and Weaver (1970) and at 5 700 MPa from Weidner and Li (2015). Clinopyroxene synthetics from Moghadam et al. (2010). Synthetic mantle rocks from Jin et al. (2001). Rotational flattening from Eq. (19). Stress from circulation is obtained from Eq. (8) plate velocities. Even if velocities are $\times 50$ larger, the drag force is still within the elastic regime (grey field for high-temperature behavior), as defined by trends in the data.

$$\kappa = \lambda^2/\tau = u_{\text{micro}}\lambda = u_{\text{macro}}h \quad (15)$$

where u_{macro} is the speed of the cooling front. Because κ is a material property, and therefore is independent of size, the product of speed times distance during the flow of heat is invariant (Hofmeister, 2010).

Substituting the mass self-diffusion coefficient (D_m) for κ and concentration for T in Eq. (14) generates Fick's equation for mass diffusion: $\partial c_i / \partial t = D_{m,i} \nabla^2 c_i$ where c is a concentration and i designates a species. Consequently, a formula for mass diffusion that is analogous to Eq. (15) exists.

High κ (or D_m) indicate rapid flow of heat (or mass), whereas high v indicates slow flow of matter. This contrast exists because momentum is not governed by an equation analogous to Eq. (14), but instead is governed by Eq. (8). That other, more complicated formula for non-Newtonian fluids may pertain is immaterial: viscosity in condensed matter describes the resistance of a material to imposed stress. Obviously, kinematic viscosity cannot describe the diffusion of momentum in general. This incorrect analogy has been made in many works, due to behavior that is unique to the gaseous state of matter, as follows.

Gas behavior has been the focus of thermodynamics (e.g. Fegley, 2015) and of heat transfer models (reviewed by Hofmeister and Branlund, 2016). Importantly, gas is the only state of matter wherein heat and mass are diffused by the same carrier (the molecules, Fig. 3a). Due to molecular motions being the sole means of transport in gas, their transport properties are equal in the kinetic theory of gas, developed by Clausius and Maxwell in the mid-1800s (e.g., Reif, 1965). Experiments on gas, even if nearly ideal (e.g., He in Table 3) show instead that

$$\kappa = D_m \sim 3v/2 \quad (16)$$

Thus, diffusion of momentum does not precisely describe gases. Because kinetic theory assumes elastic interactions, deformation of the gas molecules during collisions is not accounted for.

Physical properties of pourable liquids occupy a restricted range of values about this gas line, whereas solids greatly diverge (Fig. 9). This situation arises because for liquids, most heat is carried by molecules, although some heat is transported by their internal vibrations (Fig. 3b). Thus, liquids can be approximated by gas behavior. In great contrast, for ionic solids, heat is entirely associated with interatomic vibrations (Fig. 4) whereas creep at low stress occurs via atomic diffusion (e.g., Meyers and Chawla, 2009). Consequently, κ , v and D_m of solids differ enormously (Table 3, Fig. 9). The diverse substances presented in Table 3 include mantle candidate materials, and substances for which stability limits have been probed, and illustrate the wide range of possible behaviors for gas, liquid, and solids. Diffusion of heat by vibrations far outpaces atomic diffusion in solids because the former does not require breaking and reforming the strong, interatomic bonds.

The Lewis number describes the competition of the two diffusive processes

$$Le = \pi_8 = \kappa/D_m \quad (17)$$

When Le is large, the thermal advantage of a hot particle in a

creeping solid is removed faster than that particle can possibly rise.

3.5 Stability Criteria from Combining Force Balance and Diffusive Mitigation

Vigor of flow in solids above their yield stress depends on the force balance of Eq. (10). Because heat and mass flow are decoupled in solids, each force is mitigated by the relevant diffusion coefficient. Instability exists when

$$\frac{F_{\text{buoyancy}}}{F_{\text{drag}}} \frac{D_m}{\kappa} > 1; \text{ i.e., } \frac{Gr}{Le} > 1; \text{ or } \frac{Ra}{Sc} > 1 \quad (18)$$

where the Schmidt number is $Sc = v/D_m$, and the Ra is that modified to include yield strength effects. Although derived by considering the behavior of solids, Eq. (18) leads to $Ra_{\text{critical}} \sim 1\,000$ for simple liquids, which have Sc near 1 000 (Table 3). Furthermore, using Eq. (16) which describes gas provides critical Gr and Ra of unity. This deduction is supported by experiments: a gas convects when the adiabatic gradient is exceeded.

For a solid close to the yield point, the ratio of buoyant to resistive forces is near unity, i.e., $Gr \sim 1$. Thus, the flow criterion simplifies to $Le < 1$, which is not observed in solids (Fig. 9). Although creep can occur in solids, the much faster process of thermal diffusion overwhelms such behavior.

3.6 Temperature Gradients and Stability

For the atmosphere, stability exists as long as the temperature gradient is subadiabatic. As with simple gasses, the thermodynamically controlled isentropic gradient can be substituted for the adiabat (Sec. 1.2). This substitution is possible because mass and heat in gases move by the same mechanism, leading to a simple equation of state. Critically, solids do not behave like gases, because heat and mass move independently. These dissimilarities are even more significant for planets, because the temperature gradient inside a planet is not adiabatic, due to internal heat sources (Sec. 0).

For solids, an alternative exists to convective instability, namely, when a solid becomes too hot, it melts. In the laboratory, a solid will stably conduct heat as long as the imposed temperature gradient does not exceed the melting temperature in any region. If the gradient causes melting, this phase is more buoyant and far less viscous than the solid. The Ra formulation does not describe variable properties, let alone a two phase system. Thus, large Ra for a solid implicitly assumes that melting is not involved.

3.7 Revised Stability Relations Combined and Evaluated

This section summarizes and combines the findings in the previous sections and subsections. We discuss our results in view of the available data on large bodies and relevant materials.

From Section 2, a geometrical modification is needed to apply the dimensionless Ra , Gr , and Nu numbers to planets: this stems from mass conservation (continuity). For self-gravitating bodies, which are generally nearly spherical, the classical Ra number must be multiplied by π_6^3 and the classical Nu must be multiplied by π_6 , as defined in Eq. (6). This π -group introduces a surface radius term to the dimensionless Ra . As such, this

Table 3 Diffusivity and viscosity data

Substance	T (°C)	κ (mm ² ·s ⁻¹)	D_m (mm ² ·s ⁻¹)	ν (mm ² ·s ⁻¹)	Ra_{crit}	Refs.
H ₂	25	160	160	128		a, b, c
Helium	25	190	139	110		a, b, c
Air or N ₂	25	16	15.5	15.7		a, b, c
Argon	25	18	15	12		d
Xenon	25	5.4	4.8	3.6		d
Water	25	0.14	0.002	1.0	1 760	a, b, e, f
Ethanol	RT	0.081	0.000 84	1.52		b, f, g
Benzene	RT	0.095	0.002 2	0.7		a, f
Honey	25	0.093		74		b, h
Soy oil	38	0.075		35		i, j
Olive oil	25	0.071	6.5×10 ⁻⁵	80		i, k, l
Sunflower oil	38	0.056	4.1×10 ⁻⁵	66		i, k, l
Palm oil	RT	0.12	1.1×10 ⁻⁵	100		j, k, m
Engine oil SAE 40	100	0.073 8		12		a, b
Tar	100	0.50		560		b, n
Glycerol	100	0.10	5×10 ⁻⁶	1 100	1 580	e, o
Ethyleneglycol	RT	0.093 8		17.8		b, g
Vinegar	20	0.076	0.001 2	1.14		f, p
Lyle's golden syrup	20	0.122		22 000	1 690	q
Silicone oil	RT	0.101		21	1 750	r
Silicone oil	RT	0.098		50	1 741	r
Silicone oil	RT	0.11	1.16×10 ⁻⁵	100	1 630	r, s
Silicone oil	RT	0.12	3.49×10 ⁻⁶	200	1 675	r, s
Mercury liquid	RT	4.0	0.001 6	0.11	1 680	b, t
Gallium liquid	20	10	0.001 8	0.32	2 320	u
Zn ₆₄ Ni ₃₆ melt	1 556	10	0.000 78	3.63	-	v
Zn ₆₄ Ni ₃₆ melt	1 923	11.0	0.002 3	1.16	-	v
Zn ₆₄ Ni ₃₆ alloy	1 377	12.0	0.000 23	14.5	-	v
Silica melt	2 100	0.45		4×10 ⁶	-	w
Silica glass	1 300	0.70	2×10 ⁻⁵ (O ₂)	7×10 ¹²	-	w, x
Rhyolite melt	1 400	0.52	5×10 ⁻⁹ (O)	1.3×10 ⁷	-	x, y
Rhyolite glass	1 000	0.55	10 ⁻¹³	2×10 ¹⁵	-	x, y
Basalt melt	1 200	0.29	5×10 ⁻⁶	200 000	-	x, z
Basalt glass	700	0.45	8×10 ⁻⁹	1×10 ¹²	-	x, z
Olivine/mantle	1 000	1.0	10 ⁻¹³	10 ²⁰ -10 ²³	-	aa

Notes: RT=room temperature. a. For κ , common substances and references are listed at https://en.wikipedia.org/wiki/Thermal_diffusivity; b. for ν of many substances, see http://www.engineeringtoolbox.com/kinematic-viscosity-d_397.html; c. for D_m of gas, see Cussler (2008) or <http://www.thermopedia.com/content/696/>; d. see Kestin et al. (1984) and https://en.wikipedia.org/wiki/Noble_gas; e. He et al. (2006); f. for D_m of many liquids, see Ertl and Dullien (1973) and also Cussler (2008); g. Huang and Liu (2009); h. Nguyen et al. (2012); i. Yáñez-Limón et al. (2005); j. Coupland and McClements (1997); k. Xu et al. (2014); l. Diamante and Lan (2014); m. de Freitas Cabral et al. (2011); n. Luca and Mrawira (2005); o. Stengel et al. (1982); p. Bleazard et al. (1996); q. White (1988); r. Koschmieder and Pallas (1974); s. Thern and Lüdemann (1996); t. Schriempf (1972); Meyer (1961); u. Schriempf (1973); Blagoveshchenskii et al. (2015); Aurnou and Olson (2001); v. Brillo et al. (2011); κ estimated from Ni data by Nishi et al. (2003); w. Hofmeister and Whittington (2012); Doremus (2002); Kajihara et al. (2005); x. Zhang et al. (2010); y. Romine et al. (2012); Romine and Whittington (2015); z. Nabelek et al. (2012); Sehlke et al. (2014); Hofmeister et al. (2016); aa. Davies (2011) lists κ and μ considered typical of the mantle from various sources; for D_m see Chakraborty (2010).

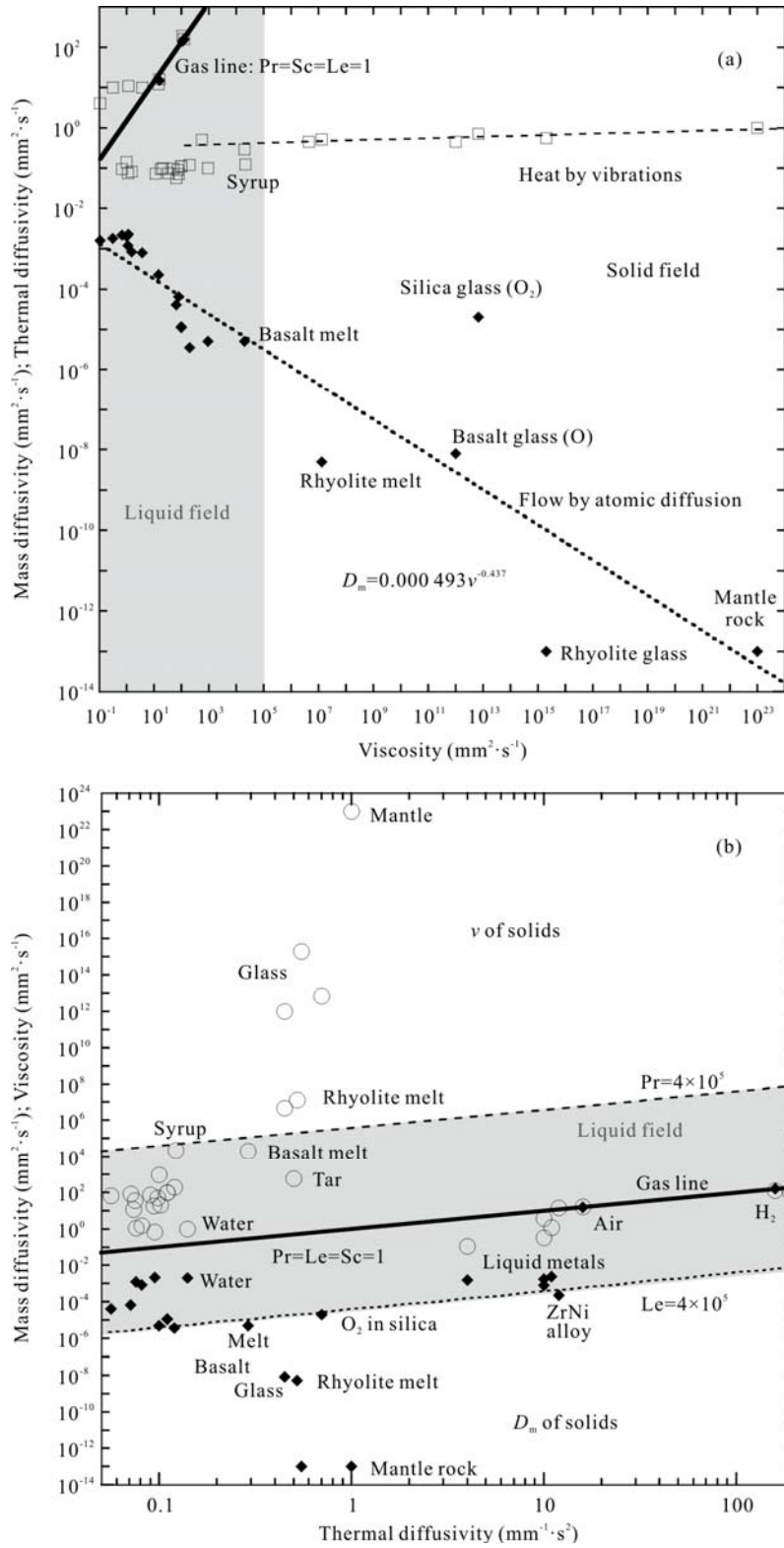


Figure 9. Regimes of transport properties, focusing on common substances and Earth materials. Data from Table 3. κ (Squares), D_m (diamonds), ν (circles). Some substances are labeled. Heavy solid line. gas trend with $D_m=\kappa=\nu$; grey area. liquids, where the boundaries with solids were estimated from whether a fluid pores, even if slowly. (a) Diffusion properties against viscosity. Dashed line=vibrational heat transport in solids. Transport of heat dominated by unimpeded molecular motions gives κ higher by a factor of >30 . If molecular motions are impeded, yet the substance is not dense enough for vibrations to easily propagate, κ is low, $\sim 0.1 \text{ mm}^2 \cdot \text{s}^{-1}$, as occurs across loosely bound layers in mica. Dotted line with fit=trend for mass diffusion for liquids and solids, combined. From the Einstein-Stokes model of liquids: $D_m=\text{constant } T/\nu$, which differs greatly from gas where $D_m=\nu$. But, $D_m=\text{constant}/\nu$ for dense liquids, glassy alloys (Brillo et al., 2011) and polyethelenes with low molecular weight (Pearson et al., 1987). (b) Viscosity and mass diffusion against thermal diffusion. Broken lines=approximate limits for pourable liquids. Liquids have properties straddling the gas line, whereas solids diverge greatly. The different behaviors result from disparate responses to applied stress and different mechanisms dominating diffusion for solids than in liquids or gases.

geometrical modification to the Ra is independent of all other considerations.

Evidence for the crucial role of surface radius is provided by main sequence stars, which are all primarily composed of hydrogen and therefore governed by the same equation of state. All other characteristics of stars (color, temperature, luminosity, and mass) are simply related to the surface radius via power laws (Zombeck, 2007). Note that these power laws are generally cast as being luminosity dependent, which is the most easily determined physical property. The actual independent variable is mass, which determines everything else, including luminosity. Furthermore, similar thermal behavior of all main sequence stars indicates that the movement of heat and mass inside these stars is similar.

Geometric modifications to Ra are required to describe conditions inside planetary bodies, but other factors pertain. Section 3 demonstrates that the classical Ra is an insufficient criterion for instability of solids in an imposed temperature gradient. The classical Rayleigh number applies only to conditions where fluid-like behavior exists. Because Ra incompletely describes solids, two additional criteria for convective instability must both be met in solids. These criteria are given in Eqs. (12) and (18). Equation (12) describes resistance of solids to deformation, which is one of the two key attributes of a solid. Equation (18) addresses the fact that flow of heat in solids occurs by a different mechanism than the flow of mass, which is the second key attribute of a solid. These findings have important implications for stability. We next discuss whether evidence exists to support these corrections.

The different mechanisms which transport mass and heat in solids leads to two adaptations of the Ra. One is revision of the original stability requirement from a single value (~ 1700) to a ratio of dimensionless numbers (Eq. 18). The second is requirement of a minimum stress (Eq. 12).

Gases, including the tall atmosphere, convect when the isentrope (reversible adiabat) is exceeded, which means the critical Ra of $\text{gas}=1$. This finding agrees with Eq. (18). Yet, the data on liquids in Table 3 do not confirm Eq. (18). Importantly, to avoid temperature dependence of the physical properties from affecting the onset of instability, these experiments involve h of about 1 mm. Restriction to small h has two implications. (1) These experiments evaluate instability of a thin layer, not of a large body. (2) By designing the experiments in this manner, the researchers have acknowledged that Ra does not predict behavior when the material properties strongly depend on temperature. A few experiments (e.g., White, 1988) use taller boxes (~ 6 cm) to evaluate the effect of viscosity depending on temperature. Viscosity strongly decreases with temperature, which increases the critical Ra for pourable syrup (White, 1988). In addition, the complexity of the convection patterns increases.

The experiments on the critical Ra confirm Eq. (18) for one case, that of the yield strength being zero (Eq. 12). Both gas and liquids flow under any stress, and both of these states of matter demonstrably convect in an imposed temperature gradient, upon meeting other conditions. Convection of materials with substantial yield strengths has not been studied. Syrup is the most viscous material studied in convection experiments:

White (1988) found that time is important in these measurements of a nearly Newtonian liquid. Existence of time dependent behavior for a material with simple, nearly Newtonian properties implies that the classical, time-independent Ra incompletely describes convection in any viscous liquid.

4 APPLICATION TO EARTH'S LOWER MANTLE

The Ra formulation is not applied to the UM+TZ to justify convection of this region (Sec. 0). The following concerns behavior of the whole and/or lower mantle inferred from dimensionless numbers.

4.1 Geometry

Equation (6) for π_6 provides a value of about $\frac{1}{2}$ for the lower mantle, which reduces Ra and Gr each by a factor of ~ 10 . This reduction is small, and unimportant relative to the other factors discussed below. However, the omission of the planetary radius from Ra means that the equations used in geodynamic models must include an additional constraint, which has not previously been explored. The mathematical modifications needed to prevent strong violations of mass conservation (continuity) in radially symmetric geodynamic models are beyond the scope of the current report.

4.2 Mantle Gr

Mantle properties (e.g., Davies, 2011; Table 3) provide $\text{Gr} < 10^{-13}$, which grossly differs from $\text{Gr} > 1$ in convecting fluids (Tritton, 1977). The small value for the mantle shows that buoyancy forces are inconsequential. Because buoyancy forces cannot induce instability, these forces cannot drive convection. As such, whole mantle circulation is highly unlikely. This conclusion contrasts with previous inferences that are based solely on the large size of Ra. Inferring convective instability for the mantle from Ra involves many canceling factors within dimensionless numbers and immense extrapolations (Table 4), and is not a reliable predictor of instability for large, planetary bodies.

4.3 Stress in the Lower Mantle

Various lines of reasoning indicate that the conditions in the lower mantle are consistent with the elastic regime.

(1) As stated by Hirth (2002) and others, nearly hydrostatic conditions prevail below ~ 10 km. Of course this finding does not hold within or adjacent to the subducting slabs, but these features are a small part of the whole mantle. Regarding the lower mantle, absence of earthquakes below ~ 670 km indicates that hydrostatic conditions prevail everywhere in the lower mantle.

(2) Yield strength increasing with pressure in the Drucker-Prager and Mohr-Coulomb yield criteria (Borosi and Schmidt, 2003) is supported by experiments (Fig. 8; Kavner and Duffy, 2001). Hence, in the lower mantle, large shearing forces are needed to move this region out of the elastic regime. Even if the slabs penetrate below 670 km, the lack of deeper earthquakes shows that this manner of indentation is insufficient to create significant amounts of stress.

(3) We estimate average effective deviatoric stress (Fig. 7) across the whole mantle relative to ΔP in two independent approaches. First, strain is induced by rotational flattening of the globe. We estimate this effect dimensionally

$$\frac{\delta\sigma}{\Delta P} \approx \frac{\delta h}{h} \quad (19)$$

Earth's equatorial radius is 23 km greater than its polar radius. Over the whole mantle, $\delta\sigma < 0.2\%$ of the pressure. This calculation provides an upper limit for the mantle because the highest deviatoric stresses actually occur inside the rigid lithosphere, and are not relevant to the elastic lower mantle. Alternatively, we can estimate drag from Eq. (8) using plate velocities, and then convert this shear to an effective stress (Fig. 7). This procedure gives a lower value (Fig. 8). Deviatoric stress in the lower mantle is therefore quite low.

(4) Frenkels' equation (e.g., Meyers and Chawla, 2009) relates the theoretical shear strength of a material to the shear modulus. Hence, the yield strength of a real material should be related to its shear modulus. In the mantle, G is large and increases with depth, suggesting great resistance of this medium

Table 4 Comparison of conditions in laboratory experiments used to ascertain critical Ra for fluids to conditions in Earth's lower mantle

Parameter	Laboratory	Mantle	Extrapolation
Gr	>1	$<10^{-13}$	$\times 10^{-13}$
Ra	$1-10^{12}$ *	$\sim 10^8$	*
Nu	$1-300$ *	$1-2$	$\times 10^{-2}-1$
Le	$100-3 \times 10^4$	$\sim 10^6$ †	$\times 10^2-10^4$ †
Sc	$500-5 \times 10^4$	$\sim 10^{36}$	$\times 10^{30}-10^{33}$
Pr	$\sim 1-10^6$ ‡	$\sim 10^{20}$	$\times 10^{14}-10^{20}$
ν	$1-10^6 \text{ mm}^2\text{s}^{-1}$	$\sim 10^{20} \text{ mm}^2\text{s}^{-1}$	$\times 10^{14}-10^{20}$
Strain rate§	$\sim 10^{-7} \text{ s}^{-1}$	$\sim 10^{-14} \text{ s}^{-1}$	$\sim \times 10^{-7}$
P	10^{-4} GPa	$>24 \text{ GPa}$	$\sim \times 10^4$
G	0	$>160 \text{ GPa}$	$\times \infty$
Effective deviatoric	$\sim 10^{-6} \text{ GPa}$ ¶	$<1\% P$	$\sim \times 10^7$
h^3	$(0.1-60 \text{ cm})^3$	$(2980 \text{ km})^3$	$\times 10^{20}-10^{28}$
Grain size	Not applicable	$\sim \text{mm-km}$	Indeterminate

Notes: Sources of parameters are listed in the figures, text, and Table 3. Not all parameters enter into the dimensionless numbers. Length-scale is cubed as used in Ra and Gr. Extrapolation refers to the order of magnitude difference between mantle and laboratory conditions. * High critical Ra experiments involve low viscosity fluids (e.g., water with Pr ~ 7 , gases with Pr ~ 1 and mercury with Pr < 1 ; Table 3), and use tall cylinders whereby Ra_{critical} depends strongly on both aspect ratio and Pr⁴ (see Glazier et al., 1999; Siggia, 1994). † If substantial radiative transport exists, this fast process ($\kappa_{\text{rad}} \sim 10^5 \times \kappa_{\text{lat}}$; Hofmeister, 2010) greatly increases Le, making heat transfer effectively instantaneous, and Ra irrelevant to the mantle. ‡ High Ra experiments involving high Pr are electrochemical with limited exploration of oils, which from Table 3 do not have high viscosity (see review by Siggia, 1994). Experiments on material with fairly high ν (e.g., syrup by White, 1988) probed much lower Ra, $< 10^5$. § These strain rates are used during deformation in solids. To determine viscosity in glasses and silicate melts, much faster rates ($\sim 1 \text{ s}^{-1}$) are used (Fig. 8; Sehlke et al., 2014), making this extrapolation considerably larger. This property is included because concerns have been previously voiced. ¶ The low stress pertains to fluid experiments, wherein Ra_{crit} was measured. A high value of $\sim 3 \text{ GPa}$ has been explored in deformation of solids, which does not involve convection.

to shear and stress.

(5) Seismic wave attenuation does not mandate viscoelastic behavior of the lower mantle because elastic materials always attenuate vibrations (Zener, 1938). Attenuation models include further ambiguities due to layering. Of particular concern is that melt is associated with strong damping. The low velocity zone, which spans depths of ~ 100 to $\sim 280 \text{ km}$, is a ductile region that has been associated with partial melting (Anderson, 1989). Because this region lies close to the surface, it is traversed by virtually all the seismic waves. Therefore, the low velocity zone could disproportionately attenuate seismic waves.

5 DISCUSSION AND CONCLUSIONS

Applying the Ra criterion for fluids to Earth's whole mantle, which is solid, involves enormous extrapolations (Table 4). Tradeoffs in multiplied parameters make this application a "sloppy model" (Transtrum et al., 2015).

Critically, solids experience significant, additional forces during lattice deformation. To address this fundamental difference, we provide additional criteria for solids. If Eq. (12) is met inside planets, Gr is reduced by π_6^3 . However, for the mantle, $Le > 10^6$ (Table 4), and so Eq. (12) is not met. In addition, the forces are roughly in balance under elastic or creep conditions, so Eq. (18) is not met. Convection of the lower or whole mantle requires buoyancy forces to exceed drag forces by $\times 10^6-10^{11}$, in order for creep to outpace the mitigating effect of thermal diffusion. Extremely high buoyancy forces would be associated with deviatoric stresses exceeding our estimate by several orders of magnitude. Such immense deviatoric stresses further implying catastrophic failure. Instead, the lower mantle is characterized by hydrostatic conditions and the absence of earthquakes.

Simplistic analogies between creep and viscous flow have obfuscated fundamental, physical differences. Unlike solids, liquids are capable of flowing under any shear stress and experiencing unlimited deformation. Equations for creep in solids only apply to a limited regime of solid behavior, and do not indicate that the solid mantle is capable of repeated circulation implied by current convection models. Hiraga et al. (2010) pointed out this problem, based on his deformation studies. We emphasize that deformation of rocks requires not only high stress, but strain rates in the laboratory far exceed rates surmised from plate velocities or glacial rebound. It is well-known that different mechanisms exist at different conditions, and that laboratory experiments differ in important ways from those of the Earth. It cannot be proven that the experiments are relevant to the Earth.

The Ra formulation describes a situation where average physical properties and a linear temperature gradient are reasonable approximations. Solids melt upon reaching high temperatures, and moreover the properties of liquids and solids of the same chemical composition vary greatly. Thus, even if the Ra were valid for solids, its use further assumes that melt production is insignificant. Yet, lubricating melt exists almost globally beneath the plates. Because buoyant melts carry latent and thermally stored heat upwards, melt production and ascent is the important process in mantle evolution, rather than whole mantle convection (see Criss and Hofmeister, 2016; Hofmeister

and Criss, 2013).

Our findings of a stable lower mantle are based on fundamental equations from thermodynamics, fluid dynamics, and continuum mechanics, which are coupled with key observations from mineral physics and seismology. Our results are compatible with conductive cooling models of the lower mantle (Criss and Hofmeister, 2016), and do not require perpetual superplasticity to describe lower mantle behavior.

Plate tectonics describes slow ($\sim 2 \text{ cm}\cdot\text{y}^{-1}$) motions of the upper $\sim 100 \text{ km}$ of rigid lithosphere. Motions below the plates cannot be discerned, and need not even exist because the underlying partial melt is essentially global and would provide lubrication for the plates to slide on. The low velocity zone immediately below the plates could be under high shear strain, because of the presence of partial melt intermixed with plastic regions. For these reasons, mantle circulation is not required to describe the behavior of the Earth, and the classical Ra number is irrelevant to planetary bodies. A mechanism specifically describing how plate tectonics operates is beyond the scope of the present report.

ACKNOWLEDGMENTS

Support for AMH was provided by NSF (No. EAR-1524495). The authors declare that no conflict of interest exists. Any opinions, findings, and conclusions or recommendations expressed in this material are those of the authors and do not necessarily reflect the views of the National Science Foundation. E. M. Criss is an employee of Panasonic Avionics Corporation, but prepared this article independent of his employment and without use of information, resources, or other support from Panasonic Avionics Corporation. The final publication is available at Springer via <https://doi.org/10.1007/s12583-017-0819-4>.

REFERENCES CITED

- Agee, C. B., 1998. Phase Transformations and Seismic Structure in the Upper Mantle and Transition Zone. *Reviews in Mineralogy*, 37: 165–204
- Anderson, D. L., 1989. *Theory of the Earth*. Blackwell Scientific, Boston
- Armienti, P., Gasperini, D., 2010. Isotopic Evidence for Chaotic Imprint in Upper Mantle Heterogeneity. *Geochemistry, Geophysics, Geosystems*, 11(5): Q0AC02. <https://doi.org/10.1029/2009gc002798>
- Aurnou, J. M., Olson, P. L., 2001. Experiments on Rayleigh–Bénard Convection, Magnetoconvection and Rotating Magnetoconvection in Liquid Gallium. *Journal of Fluid Mechanics*, 430: 283–307. <https://doi.org/10.1017/s0022112000002950>
- Bercovici, D., 2015. Mantle Dynamics: An Introduction and Overview. In: Schubert, G., ed., *Treatise on Geophysics*, 7: 1–22
- Birch, J. M., Wilshire, B., 1974. Transient and Steady State Creep Behaviour of Polycrystalline MgO. *Journal of Materials Science*, 9(6): 871–875. <https://doi.org/10.1007/bf00570377>
- Blagoveshchenskii, N., Novikov, A., Puchkov, A., et al., 2015. Self-Diffusion in Liquid Gallium and Hard Sphere Model. *EPJ Web of Conferences*, 83: 02018. <https://doi.org/10.1051/epjconf/20158302018>
- Bleazard, J. G., Sun, T. F., Teja, A. S., 1996. The Thermal Conductivity and Viscosity of Acetic Acid-Water Mixtures. *International Journal of Thermophysics*, 17(1): 111–125. <https://doi.org/10.1007/bf01448214>
- Boresi, A. P., Schmidt, R. J., 2003. *Advanced Mechanics of Materials*. John Wiley and Sons, Hoboken, NJ
- Bridgeman, P., 1927. *Dimensional Analysis*. Yale University Press, New Haven
- Brillo, J., Pommrich, A. I., Meyer, A., 2011. Relation between Self-Diffusion and Viscosity in Dense Liquids: New Experimental Results from Electrostatic Levitation. *Physical Review Letters*, 107(16): 165902. <https://doi.org/10.1103/physrevlett.107.165902>
- Buckingham, E., 1914. On Physically Similar Systems; Illustrations of the Use of Dimensional Equations. *Physical Review*, 4(4): 345–376. <https://doi.org/10.1103/physrev.4.345>
- Bürgmann, R., Dresen, G., 2008. Rheology of the Lower Crust and Upper Mantle: Evidence from Rock Mechanics, Geodesy, and Field Observations. *Annual Review of Earth and Planetary Sciences*, 36(1): 531–567. <https://doi.org/10.1146/annurev.earth.36.031207.124326>
- Carslaw, H. S., Jaeger, J. C., 1959. *Conduction of Heat in Solids*, 2nd Edition. Oxford University Press, New York
- Chakraborty, S., 2010. Diffusion Coefficients in Olivine, Wadsleyite and Ringwoodite. *Reviews in Mineralogy and Geochemistry*, 72(1): 603–639. <https://doi.org/10.2138/rmg.2010.72.13>
- Chudinovskikh, L., Boehler, R., 2007. Eutectic Melting in the System Fe-S to 44 GPa. *Earth and Planetary Science Letters*, 257(1/2): 97–103. <https://doi.org/10.1016/j.epsl.2007.02.024>
- Costin, L. S., 1985. Damage Mechanics in the Post-Failure Regime. *Mechanics of Materials*, 4(2): 149–160. [https://doi.org/10.1016/0167-6636\(85\)90013-4](https://doi.org/10.1016/0167-6636(85)90013-4)
- Coupland, J. N., McClements, D. J., 1997. Physical Properties of Liquid Edible Oils. *Journal of the American Oil Chemists' Society*, 74(12): 1559–1564. <https://doi.org/10.1007/s11746-997-0077-1>
- Criss, E. M., Smith, R. J., Meyers, M. A., 2015. Failure Mechanisms in Cobalt Welded with a Silver-Copper Filler. *Materials Science and Engineering: A*, 645: 369–382. <https://doi.org/10.1016/j.msea.2015.07.094>
- Criss, R. E., Hofmeister, A. M., 2016. Conductive Cooling of Spherical Bodies with Emphasis on the Earth. *Terra Nova*, 28(2): 101–109. <https://doi.org/10.13039/100000001>
- Cussler, E. L., 2008. *Diffusion: Mass Transport in Fluid Systems*. Cambridge University Press, Cambridge
- Davies, G. F., 2011. *Mantle Convection for Geologists*. Cambridge University Press, Cambridge
- Davis, R. O., Selvadurai, A. P. S., 2005. *Plasticity and Geomechanics*. Cambridge University Press, Cambridge
- de Freitas Cabral, A. J., de Oliveira, P. C., Moreira, S. G. C., et al., 2011. Thermal Diffusivity of Palm Olein and Compounds Containing β -Carotene. *International Journal of Thermophysics*, 32(9): 1966–1972. <https://doi.org/10.1007/s10765-011-1059-y>
- Diamante, L. M., Lan, T. Y., 2014. Absolute Viscosities of Vegetable Oils at Different Temperatures and Shear Rate Range of 64.5 to 4 835 s^{-1} . *Journal of Food Processing*, 2014(3): 1–6. <https://doi.org/10.1155/2014/234583>
- Doglionni, C., Anderson, D. L., 2015. Top Driven Asymmetric Mantle Convection. In: Foulger, G. R., Lustrino, M., King, S. D., eds., *The Interdisciplinary Earth: In Honor of Don L. Anderson. GSA Special Papers*, 214: 51–64
- Doglionni, C., Panza, G., 2015. Polarized Plate Tectonics. *Advances in Geophysics*, 56: 1–167
- Domínguez-Rodríguez, A., Gómez-García, D., Zapata-Solvas, E., et al., 2007. Making Ceramics Ductile at Low Homologous Temperatures. *Scripta Materialia*, 56(2): 89–91. <https://doi.org/10.1016/j.scriptamat.2006.09.024>
- Doremus, R. H., 2002. Viscosity of Silica. *Journal of Applied Physics*, 92(12): 7619–7629. <https://doi.org/10.1063/1.1515132>

- Du, Z., Vinnik, L. P., Foulger, G. R., 2006. Evidence from P-to-S Mantle Converted Waves for a Flat “660-km” Discontinuity beneath Iceland. *Earth and Planetary Science Letters*, 241(1/2): 271–280. <https://doi.org/10.1016/j.epsl.2005.09.066>
- Dziewonski, A. M., Anderson, D. L., 1981. Preliminary Reference Earth Model. *Physics of the Earth and Planetary Interiors*, 25(4): 297–356. [https://doi.org/10.1016/0031-9201\(81\)90046-7](https://doi.org/10.1016/0031-9201(81)90046-7)
- Elder, J., 1976. *The Bowels of the Earth*. Oxford University Press, Oxford. ISBN 0-19-854413-8
- Ertl, H., Dullien, F. A. L., 1973. Self-Diffusion and Viscosity of some Liquids as a Function of Temperature. *AIChE Journal*, 19(6): 1215–1223. <https://doi.org/10.1002/aic.690190619>
- Fegley, B. Jr., 2015. *Practical Chemical Thermodynamics for Geoscientists*. Academic Press/Elsevier, Waltham, Massachusetts
- Fichtner, A., Villaseñor, A., 2015. Crust and Upper Mantle of the Western Mediterranean—Constraints from Full-Waveform Inversion. *Earth and Planetary Science Letters*, 428: 52–62. <https://doi.org/10.1016/j.epsl.2015.07.038>
- Foulger, G. R., 2010. *Plates vs Plumes: A Geological Controversy*. Wiley-Blackwell, ISBN 978-1-4443-3679-5. 328
- Foulger, G. R., Panza, G. F., Artemieva, I. M., et al., 2013. Caveats on Tomographic Images. *Terra Nova*, 25: 259–281
- Foulger, G. R., Pritchard, M. J., Julian, B. R., et al., 2001. Seismic Tomography Shows that Upwelling beneath Iceland is Confined to the Upper Mantle. *Geophysical Journal International*, 146(2): 504–530. <https://doi.org/10.1046/j.0956-540x.2001.01470.x>
- French, S. W., Romanowicz, B., 2015. Broad Plumes Rooted at the Base of the Earth’s Mantle beneath Major Hotspots. *Nature*, 525(7567): 95–99. <https://doi.org/10.1038/nature14876>
- Frenkel, J., 1926. Zur Theorie Der Elastizitätsgrenze Und Der Festigkeit Kristallinischer Körper. *Zeitschrift für Physik*, 37(7/8): 572–609. <https://doi.org/10.1007/bf01397292>
- Gando, A., Gando, Y., Ichimura, K., et al., 2011. Partial Radiogenic Heat Model for Earth Revealed by Geoneutrino Measurements. *Nature Geoscience*, 4(9): 647–651. <https://doi.org/10.1038/ngeo1205>
- Gao, S. S., Liu, K. H., 2014. Imaging Mantle Discontinuities Using Multiply-Reflected P-to-S Conversions. *Earth and Planetary Science Letters*, 402: 99–106. <https://doi.org/10.13039/501100004342>
- Gasparik, T., 2000. Evidence for the Transition Zone Origin of some [Mg,Fe]O Inclusions in Diamonds. *Earth and Planetary Science Letters*, 183(1/2): 1–5. [https://doi.org/10.1016/s0012-821x\(00\)00254-5](https://doi.org/10.1016/s0012-821x(00)00254-5)
- Glazier, J. A., Segawa, T., Naert, A., et al., 1999. Evidence against ‘Ultra-hard’ Thermal Turbulence at very High Rayleigh Numbers. *Nature*, 398(6725): 307–310. <https://doi.org/10.1038/18626>
- Goes, S., Agrusta, R., van Hunen, J., et al., 2017. Subduction-Transition Zone Interaction: A Review. *Geosphere*, 13(3): 644–664. <https://doi.org/10.1130/ges01476.1>
- Hamilton, W. B., 2002. The Closed Upper-Mantle Circulation of Plate Tectonics. In: Stein S., Freymueller, J. T., eds., *Plate Boundary Zones: Geodynamics Series*. American Geophysical Union, Washington, D.C.. 359–410
- Hamilton, W. B., 2011. Plate Tectonics Began in Neoproterozoic Time, and Plumes from Deep Mantle have never Operated. *Lithos*, 123(1/2/3/4): 1–20. <https://doi.org/10.1016/j.lithos.2010.12.007>
- Hamilton, W. B., 2015. Terrestrial Planets Fractionated Synchronously with Accretion, but Earth Progressed through Subsequent Internally Dynamic Stages whereas Venus and Mars have been Inert for more than 4 Billion Years. *GSA Special Papers*, 514: 123–156
- Hamza, V. M., 2013. Global Heat Flow without Invoking “Kelvin Paradox”. *Frontiers in Geosciences*, 1: 11–20
- He, X. M., Fowler, A., Toner, M., 2006. Water Activity and Mobility in Solutions of Glycerol and Small Molecular Weight Sugars: Implication for Cryo- and Lyopreservation. *Journal of Applied Physics*, 100(7): 074702. <https://doi.org/10.1063/1.2336304>
- Heap, M. J., Baud, P., Meredith, P. G., et al., 2011. Brittle Creep in Basalt and Its Application to Time-Dependent Volcano Deformation. *Earth and Planetary Science Letters*, 307(1/2): 71–82. <https://doi.org/10.1016/j.epsl.2011.04.035>
- Heep, M. J., 2009. *Creep: Time-Dependent Brittle Deformation in Rocks*: [Dissertation]. University College London, London
- Henderson, G., 1982. *Inorganic Geochemistry*. Pergamon Press, New York. ISBN 0-08-020448-1
- Hetényi, G., 2014. To Conserve or not to Conserve (Mass in Numerical Models). *Terra Nova*, 26(5): 372–376. <https://doi.org/10.1111/ter.12109>
- Hill, R., 1950. *The Mathematical Theory of Plasticity*. Oxford University Press, Oxford
- Hiraga, T., Miyazaki, T., Tasaka, M., et al., 2010. Mantle Superplasticity and Its Self-Made Demise. *Nature*, 468(7327): 1091–1094. <https://doi.org/10.1038/nature09685>
- Hirth, G., 2002. Laboratory Constraints on the Rheology of the Upper Mantle. *Reviews in Mineralogy and Geochemistry*, 51(1): 97–120. <https://doi.org/10.2138/gsrmg.51.1.97>
- Hofmeister, A. M., 2010. Scale Aspects of Heat Transport in the Diamond Anvil Cell, in Spectroscopic Modeling, and in Earth’s Mantle: Implications for Secular Cooling. *Physics of the Earth and Planetary Interiors*, 180(3/4): 138–147. <https://doi.org/10.1016/j.pepi.2009.12.006>
- Hofmeister, A. M., Branlund, J. M., 2016. Thermal Conductivity of the Earth. In: Schubert, G., ed., *Treatise in Geophysics*, 2nd Edition. V. 2 Mineral Physics (Price, G. D., ed.) Elsevier, The Netherlands. 584–608
- Hofmeister, A. M., Criss, R. E., 2005. Earth’s Heat Flux Revised and Linked to Chemistry. *Tectonophysics*, 395(3/4): 159–177. <https://doi.org/10.1016/j.tecto.2004.09.006>
- Hofmeister, A. M., Criss, R. E., 2012. A Thermodynamic and Mechanical Model for Formation of the Solar System via 3-Dimensional Collapse of the Dusty Pre-Solar Nebula. *Planetary and Space Science*, 62(1): 111–131. <https://doi.org/10.13039/100000104>
- Hofmeister, A. M., Criss, R. E., 2013. How Irreversible Heat Transport Processes Drive Earth’s Interdependent Thermal, Structural, and Chemical Evolution. *Gondwana Research*, 24(2): 490–500. <https://doi.org/10.1016/j.gr.2013.02.009>
- Hofmeister, A. M., Criss, R. E., 2015. Evaluation of the Heat, Entropy, and Rotational Changes Produced by Gravitational Segregation during Core Formation. *Journal of Earth Science*, 26(1): 124–133. <https://doi.org/10.1007/s12583-015-0509-z>
- Hofmeister, A. M., Sehlke, A., Avard, G., et al., 2016. Transport Properties of Glassy and Molten Lavas as a Function of Temperature and Composition. *Journal of Volcanology and Geothermal Research*, 327: 330–348. <https://doi.org/10.13039/100000001>
- Hofmeister, A. M., Whittington, A. G., 2012. Effects of Hydration, Annealing, and Melting on Heat Transport Properties of Fused Quartz and Fused Silica from Laser-Flash Analysis. *Journal of Non-Crystalline Solids*, 358(8): 1072–1082. <https://doi.org/10.1016/j.jnoncrysol.2012.02.012>
- Huang, L. H., Liu, L. S., 2009. Simultaneous Determination of Thermal Conductivity and Thermal Diffusivity of Food and Agricultural Materials Using a Transient Plane-Source Method. *Journal of Food Engineering*, 95(1): 179–185. <https://doi.org/10.1016/j.jfoodeng.2009.04.024>
- Jin, Z. M., Zhang, J. F., Green, H. W. II, et al., 2001. Eclogite Rheology: Implications for Subducted Lithosphere. *Geology*, 29(8): 667–670.

- [https://doi.org/10.1130/0091-7613\(2001\)029<0667:erifsl>2.0.co;2](https://doi.org/10.1130/0091-7613(2001)029<0667:erifsl>2.0.co;2)
- Kajihara, K., Kamioka, H., Hirano, M., et al., 2005. Interstitial Oxygen Molecules in Amorphous SiO₂. III. Measurements of Dissolution Kinetics, Diffusion Coefficient, and Solubility by Infrared Photoluminescence. *Journal of Applied Physics*, 98(1): 013529. <https://doi.org/10.1063/1.1943506>
- Kavner, A., Duffy, T. S., 2001. Strength and Elasticity of Ringwoodite at Upper Mantle Pressures. *Geophysical Research Letters*, 28(14): 2691–2694. <https://doi.org/10.1029/2000gl012671>
- Kestin, J., Knierim, K., Mason, E. A., et al., 1984. Equilibrium and Transport Properties of the Noble Gases and Their Mixtures at Low Density. *Journal of Physical and Chemical Reference Data*, 13(1): 229–303. <https://doi.org/10.1063/1.555703>
- Kohlstedt, D. L., Hansen, L. N., 2015. Constitutive Behavior, Rheological Behavior, and Viscosity of Rocks. In: Schubert, G., ed., *Treatise in Geophysics*, 2nd Edition, Vol. 2. Elsevier, The Netherlands. 389–427
- Koschmieder, E. L., Pallas, S. G., 1974. Heat Transfer through a Shallow, Horizontal Convecting Fluid Layer. *International Journal of Heat and Mass Transfer*, 17(9): 991–1002. [https://doi.org/10.1016/0017-9310\(74\)90181-1](https://doi.org/10.1016/0017-9310(74)90181-1)
- Langdon, T. G., 1982. Fracture Processes in Superplastic Flow. *Metal Science*, 16(4): 175–183. <https://doi.org/10.1179/030634582790427208>
- Lodders, K., 2000. An Oxygen Isotope Mixing Model for the Accretion and Composition of Rocky Planets. *Space Science Review*, 92: 341–354
- Luca, J., Mrawira, D., 2005. New Measurement of Thermal Properties of Superpave Asphalt Concrete. *Journal of Materials in Civil Engineering*, 17(1): 72–79. [https://doi.org/10.1061/\(asce\)0899-1561\(2005\)17:1\(72\)](https://doi.org/10.1061/(asce)0899-1561(2005)17:1(72))
- Meyer, R. E., 1961. Self-Diffusion of Liquid Mercury. *The Journal of Physical Chemistry*, 65(3): 567–568. <https://doi.org/10.1021/j100821a507>
- Meyers, M. A., Chawla, K. K., 2009. *Mechanical Behavior of Materials*. Cambridge University Press, Cambridge
- Mitchell, B. S., 2004. *An Introduction to Materials Engineering and Science for Chemical and Materials Engineers*. John Wiley and Sons, Inc., Hoboken
- Moghadam, R. H., Trepmann, C. A., Stöckhert, B., et al., 2010. Rheology of Synthetic Omphacite Aggregates at High Pressure and High Temperature. *Journal of Petrology*, 51(4): 921–945. <https://doi.org/10.1093/petrology/egq006>
- Mukherjee, A. K., Bird, J. E., Dorn, J. E., 1969. Experimental Correlation for High-Temperature Creep. *Transactions of the American Society of Metals*, 62: 155–179
- Nabelek, P. I., Hofmeister, A. M., Whittington, A. G., 2012. The Influence of Temperature-Dependent Thermal Diffusivity on the Conductive Cooling Rates of Plutons and Temperature-Time Paths in Contact Aureoles. *Earth and Planetary Science Letters*, 317/318: 157–164
- Nguyen, L. T., Balasubramaniam, V. M., Sastry, S. K., 2012. Determination of In-Situ Thermal Conductivity, Thermal Diffusivity, Volumetric Specific Heat and Isobaric Specific Heat of Selected Foods under Pressure. *International Journal of Food Properties*, 15(1): 169–187. <https://doi.org/10.1080/10942911003754726>
- Nishi, T., Shibata, H., Waseda, Y., et al., 2003. Thermal Conductivities of Molten Iron, Cobalt, and Nickel by Laser Flash Method. *Metallurgical and Materials Transactions A*, 34(12): 2801–2807. <https://doi.org/10.1007/s11661-003-0181-2>
- Nishihara, Y., Tinker, D., Kawazoe, T., et al., 2008. Plastic Deformation of Wadsleyite and Olivine at High-Pressure and High-Temperature Using a Rotational Drickamer Apparatus (RDA). *Physics of the Earth and Planetary Interiors*, 170(3/4): 156–169. <https://doi.org/10.1016/j.pepi.2008.03.003>
- Paterson, M. S., 1958. Experimental Deformation and Faulting in Wombeyan Marble. *Geological Society of America Bulletin*, 69(4): 465–475. [https://doi.org/10.1130/0016-7606\(1958\)69\[465:edafiw\]2.0.co;2](https://doi.org/10.1130/0016-7606(1958)69[465:edafiw]2.0.co;2)
- Paterson, M. S., Weaver, C. W., 1970. Deformation of Polycrystalline MgO under Pressure. *Journal of the American Ceramic Society*, 53(8): 463–471. <https://doi.org/10.1111/j.1151-2916.1970.tb12678.x>
- Pearson, D. S., Ver Strate, G., Von Meerwall, E., et al., 1987. Viscosity and Self-Diffusion Coefficient of Linear Polyethylene. *Macromolecules*, 20(5): 1133–1141. <https://doi.org/10.1021/ma00171a044>
- Prewitt, C. T., Downs, R. T., 1998. High-Pressure Crystal Chemistry. *Reviews in Mineralogy*, 37: 284–342
- Rayleigh, L., 1916. On Convection Currents in a Horizontal Layer of Fluid, when the Higher Temperature is on the under Side. *Philosophical Magazine Series 6*, 32(192): 529–546. <https://doi.org/10.1080/14786441608635602>
- Rees, B. A., Okal, E. A., 1987. The Depth of the Deepest Historical Earthquakes. *Pure and Applied Geophysics*, 125(5): 699–715. <https://doi.org/10.1007/bf00878029>
- Reif, F., 1965. *Fundamentals of Statistical and Thermal Physics*. McGraw-Hill Book Company, St. Louis. 651
- Romine, W. L., Whittington, A. G., 2015. A Simple Model for the Viscosity of Rhyolites as a Function of Temperature, Pressure and Water Content. *Geochimica et Cosmochimica Acta*, 170: 281–300. <https://doi.org/10.1016/j.gca.2015.08.009>
- Romine, W. L., Whittington, A. G., Nabelek, P. I., et al., 2012. Thermal Diffusivity of Rhyolitic Glasses and Melts: Effects of Temperature, Crystals and Dissolved Water. *Bulletin of Volcanology*, 74(10): 2273–2287. <https://doi.org/10.1007/s00445-012-0661-6>
- Schriempf, J. T., 1972. A Laser Flash Technique for Determining Thermal Diffusivity of Liquid Metals at Elevated Temperatures. *Review of Scientific Instruments*, 43(5): 781–786. <https://doi.org/10.1063/1.1685757>
- Schriempf, J. T., 1973. Thermal Diffusivity of Liquid Gallium. *Solid State Communications*, 13(6): 651–653. [https://doi.org/10.1016/0038-1098\(73\)90451-1](https://doi.org/10.1016/0038-1098(73)90451-1)
- Schubert, G., Turcotte, D. L., Olson, P., 2001. *Mantle Convection in the Earth and Planets*. Cambridge University Press, Cambridge
- Sehlke, A., Whittington, A., Robert, B., et al., 2014. Pahoehoe to ‘a’a Transition of Hawaiian Lavas: An Experimental Study. *Bulletin of Volcanology*, 76(11): 876–896. <https://doi.org/10.1007/s00445-014-0876-9>
- Shimada, M., Cho, A., Yukutake, H., 1983. Fracture Strength of Dry Silicate Rocks at High Confining Pressures and Activity of Acoustic Emission. *Tectonophysics*, 96(1/2): 159–172. [https://doi.org/10.1016/0040-1951\(83\)90248-2](https://doi.org/10.1016/0040-1951(83)90248-2)
- Siggia, E. D., 1994. High Rayleigh Number Convection. *Annual Review of Fluid Mechanics*, 26(1): 137–168. <https://doi.org/10.1146/annurev.fl.26.010194.001033>
- Smith, E. M., Shirey, S. B., Nestola, F., et al., 2016. Large Gem Diamonds from Metallic Liquid in Earth’s Deep Mantle. *Science*, 354(6318): 1403–1405. <https://doi.org/10.13039/100000001>
- Soutas-Little, R., 2011. History of Continuum Mechanics. In: Merodio, J., Saccomandi, G., eds., *Continuum Mechanics*. Eolss Publishers, Singapore. 80–93
- Stacey, F. D., Stacey, C. H. B., 1999. Gravitational Energy of Core Evolution: Implications for Thermal History and Geodynamo Power. *Physics of the Earth and Planetary Interiors*, 110(1/2): 83–93. [https://doi.org/10.1016/s0031-9201\(98\)00141-1](https://doi.org/10.1016/s0031-9201(98)00141-1)

- Stein, C. A., Stein, S. A., 1992. A Model for the Global Variation in Oceanic Depth and Heat Flow with Lithospheric Age. *Nature*, 359(6391): 123–129. <https://doi.org/10.1038/359123a0>
- Stengel, K. C., Oliver, D. S., Booker, J. R., 1982. Onset of Convection in a Variable-Viscosity Fluid. *Journal of Fluid Mechanics*, 120: 411–431. <https://doi.org/10.1017/s0022112082002821>
- Them, A., Lüdemann, H. D., 1996. P, T Dependence of the Self Diffusion Coefficients and Densities in Liquid Silicone Oils. *Zeitschrift für Naturforschung A*, 51(3): 192–196. <https://doi.org/10.1515/zna-1996-0310>
- Timoshenko, S. P., Goodier, J. N., 1970. *Theory of Elasticity*. McGraw-Hill, New York
- Transtrum, M. K., Machta, B. B., Brown, K. S., et al., 2015. Perspective: Sloppiness and Emergent Theories in Physics, Biology, and beyond. *The Journal of Chemical Physics*, 143(1): 010901. <https://doi.org/10.13039/100000001>
- Tritton, D. J., 1977. *Physical Fluid Dynamics*. Van Nostrand Reinhold, New York
- Van Schmus, W. R., 1995. Natural Radioactivity of the Crust and Mantle. In: Ahrens, T. J., ed., *Global Earth Physics*. American Geophysical Union, Washington D.C. 283–291
- Wawersik, W. R., Brace, W. F., 1970. Post-Failure Behavior of a Granite and Diabase. *Rock Mechanics and Rock Engineering*, 3: 61–85
- Weidner, D. J., Li, L., 2015. Methods for the Study of High *P/T* Deformation and Rheology. In: Schubert, G., ed., *Treatise on Geophysics*, 2: 339–358
- White, D. B., 1988. The Planforms and Onset of Convection with a Temperature-Dependent Viscosity. *Journal of Fluid Mechanics*, 191: 247–286. <https://doi.org/10.1017/s0022112088001582>
- Whittington, A. G., Hofmeister, A. M., Nabelek, P. I., 2009. Temperature-Dependent Thermal Diffusivity of Earth's Crust: Implications for Crustal Anatexis. *Nature*, 458: 319–321
- Xu, Z., Morris, R., Bencsik, M., et al., 2014. Detection of Virgin Olive Oil Adulteration Using Low Field Unilateral NMR. *Sensors*, 14(2): 2028–2035. <https://doi.org/10.3390/s140202028>
- Yáñez-Limón, J. M., Mayen-Mondragón, R., Martínez-Flores, O., et al., 2005. Thermal Diffusivity Studies in Edible Commercial Oils Using Thermal Lens Spectroscopy. *Superficies y Vacío*, 18: 31–37
- Zemansky, M. W., Dittman, R. H., 1981. *Heat and Thermodynamics*, 6th Edition. McGraw-Hill, New York
- Zener, C., 1938. Internal Friction in Solids II. General Theory of Thermoeastic Internal Friction. *Physical Review*, 53(1): 90–99. <https://doi.org/10.1103/physrev.53.90>
- Zhang, Y., Ni, H., Chen, Y., 2010. Diffusion of H, C, and O Components in Silicate Melts. *Reviews in Mineralogy and Geochemistry*, 72(1): 171–225. <https://doi.org/10.2138/rmg.2010.72.5>
- Zhong, S. J., Yuen, D. A., Moresi, L. M., et al., 2015. Numerical Method for Mantle Convection. In: Schubert, G., ed., *Treatise on Geophysics. Mantle Dynamics*, 7: 197–222
- Zombeck, M. V., 2007. *Handbook of Space Astronomy and Astrophysics*. Cambridge University Press, Cambridge